Flux-Based Dynamic Subspace Model Predictive Control of Dual-Three Phase Permanent Magnet Synchronous Motors

FLUX-BASED DYNAMIC SUBSPACE MODEL PREDICTIVE CONTROL OF DUAL-THREE PHASE PERMANENT MAGNET SYNCHRONOUS MOTORS

BY

WILLIEM AGNIHOTRI, B.Eng

A THESIS

SUBMITTED TO THE DEPARTMENT OF ELECTRICAL & COMPUTER ENGINEERING

AND THE SCHOOL OF GRADUATE STUDIES

OF MCMASTER UNIVERSITY

IN PARTIAL FULFILMENT OF THE REQUIREMENTS

FOR THE DEGREE OF

Master of Applied Science

Master of Applied Science (2022) McMaster University

(Electrical & Computer Engineering) Hamilton, Ontario, Canada

TITLE:	Flux-Based Dynamic Subspace Model Predictive Control of Dual-Three Phase Permanent Magnet Synchronous Motors
AUTHOR:	Williem Agnihotri B.Eng (Electrical and Biomedical Engineering) McMaster University
SUPERVISOR:	Dr. Nahid-Mobarakeh
NUMBER OF PAGES:	xiv, 103

To my parents, who have always been supportive of me.

Abstract

Dual-three phase permanent magnet synchronous motors (DTP-PMSM) are becoming more popular in the automotive field. Their potential to increase the reliability and efficiency of the vehicle makes them an attractive replacement for the three-phase alternative. However, the increased number of phases makes the control of the machine more complex. As a result, conventional controllers can see reduced performance, especially at high speeds and torques. Currently, with the increased processing power of modern micro-controllers and field-programmable gate arrays (FPGA), many researchers are investigating whether finite-control set model predictive control (FCS-MPC) can be a suitable alternative.

FCS-MPC is simple to implement and can achieve a better dynamic performance when compared to other controllers. Furthermore, the algorithm can be augmented for specific optimization goals and non-linearities to the system, which gives the designer creativity in improving the system response. However, Model-Predictive Control suffers from a variable switching frequency as well as reduced steady-state performance. It generally has increased current ripple in the phase currents.

This thesis presents a method of reducing the steady-state ripples in FCS-MPC by introducing the use of virtual-flux in the model equations, the incremental model, and a dynamic vector search-space. All three of these applications make FCS-MPC have a

significantly improved steady-state performance when compared to the conventional algorithm, while still keeping the benefit of the improved dynamic response. The benefits of the proposed techniques techniques are verified through simulation as well as on an experimental setup.

Acknowledgements

First and foremost I would like to thank my supervisor Dr. Babak Nahid-Mobarakeh, whose expertise, patience, and guidance allowed me to have an engaging experience even during the pandemic. His teaching made my experience hundreds of times better than I expected.

Furthermore, I would like to thank Dr. Diego Valencia, who introduced me to the topic of model predictive control as well as mentored me for the majority of my studies. His input helped me greatly in my work and I am grateful for his dedication and commitment.

I would also like to thank the other members of the Stellantis Motor Control RTA as well as Stellantis itself. The members of the team were all experts in their fields, and they provided invaluable advice throughout my studies. Furthermore, without the funding from stellantis, the work would not have been able to go on.

Finally I would like to express my appreciation to the students and researchers at the McMaster Automotive Resource Centre, who provided great support in the completion of this project. The warm environment of the lab helped keep my motivation while completing my studies.

Contents

List of Tables

List of Figures

Chapter 1

Introduction

1.1 Motivation

The demand for electric vehicles has never been higher. The affects of climate change as well as rising gas prices has many people wanting an alternative fuel source [Hidrue et al.(2011)Hidrue, Parsons, Kempton, and Gardner]. In addition, many countries are expecting to phase out fully gas powered vehicles within the next 10 to 15 years [Ekta Bibra et al.(2021)Ekta Bibra, Connelly, Gorner, Lowans, Paoli, Tattini, and Teter]. As a result electric vehicle sales is expected to be 145 million globally, with an average growth rate of 30% per year. [Ekta Bibra et al.(2021)Ekta Bibra, Connelly, Gorner, Lowans, Paoli, Tattini, and Teter].

This change is not limited to just cars and trucks. There is a push in the aerospace industry for replacing the hydraulic and gas powered components with electric powered ones [Barzkar and Ghassemi(2020)]. Electric motors have a much wider operating range, have higher efficiencies at low speeds, and have a higher degree of fault tolerance, which makes them an attractive replacement, especially in the aerospace field

where continued functionality is critical.

In industry, the most popular type of motor used are AC three-phase synchronous motors. They use the interaction of magnetic fields to produce rotation [Li and Curiac(2011)]. The rotor of the motor has a magnetic field associated with it, and when another magnetic field is produced in the stator, the interaction produces torque. If one wants to have sustained rotation, a rotating magnetic field needs to be produced in the stator. This rotating field is produced by alternating current, through three phases offset in phase by 120 degrees. Using three phases allows more power to be delivered while minimizing the number of wires required.

The majority of vehicles on the market today use permanent magnets mounted on the rotor to generate it's magnetic field [Bhatt et al.(2019)Bhatt, Mehar, and Sahajwani]. These types of motors are called permanent magnet synchronous motors (PMSM). Compared to other motor types like induction or switched reluctance, PMSMs have higher efficiencies, lower torque ripples, and a higher torque density, meaning they can produce a larger output power with a smaller size [Hashemnia and Asaei(2008)]. However, conventional three phase PMSMs still have their disadvantages. They can experience reduced performance over time when exposed to high speeds, stresses, and temperatures due to the changes in flux of the permanent magnets. [Moon et al.(2016)Moon, Lee, Jeong, and Kim]. In lite of this, many researchers have suggested replacing the three-phase motors with their multi-phase counterparts [Levi(2008), Salem and Narimani(2019), Bojoi et al.(2018)Bojoi, Boggero, Comino, Fioriti, Tenconi, and Vaschetto, Liu et al.(2021)Liu, Chau, Lee, and Song]. The additional phases allow for increased reliability, greater efficiency, and enhanced robustness. Furthermore, since they require less current per phase to power

them, they reduce the size and cost of the associated power electronics. However, there is a cost associated with the increased number of phases. One would need to purchase an increased number of switches and gate drivers (commonly IGBTs are used) to power the motor. For example, with a six-phase motor, one would need double the amount of switches and gate drivers for the machine. This would increase overall price of the inverter significantly as IGBT's and the associated gate drivers can be very expensive.

In literature, the most suggested multi-phase machine for automotive applications is the asymmetrical dual-three phase machine. Asymmetrical multi-phase machines use multiple sets of three phase windings spatially shifted by $180/n$ [Liu et al.(2021)Liu, Chau, Lee, and Song, Taylor et al.(2021)Taylor, Valencia Garcia, Taha, Mohamadian, Luedtke, Nahid-Mobarakeh, Bilgin, and Emadi]. In these machines, the neutral points are isolated, which eliminates the zero-order harmonics. Furthermore, by using multiple-three phase windings, control techniques developed for three-phase machines can be easier transferred. Typically, the type of motor that is investigated in the literature is the dual-three phase motor. This machine can be seen in 1.1. The motor has two sets of three phase windings, offset by 30 degrees.

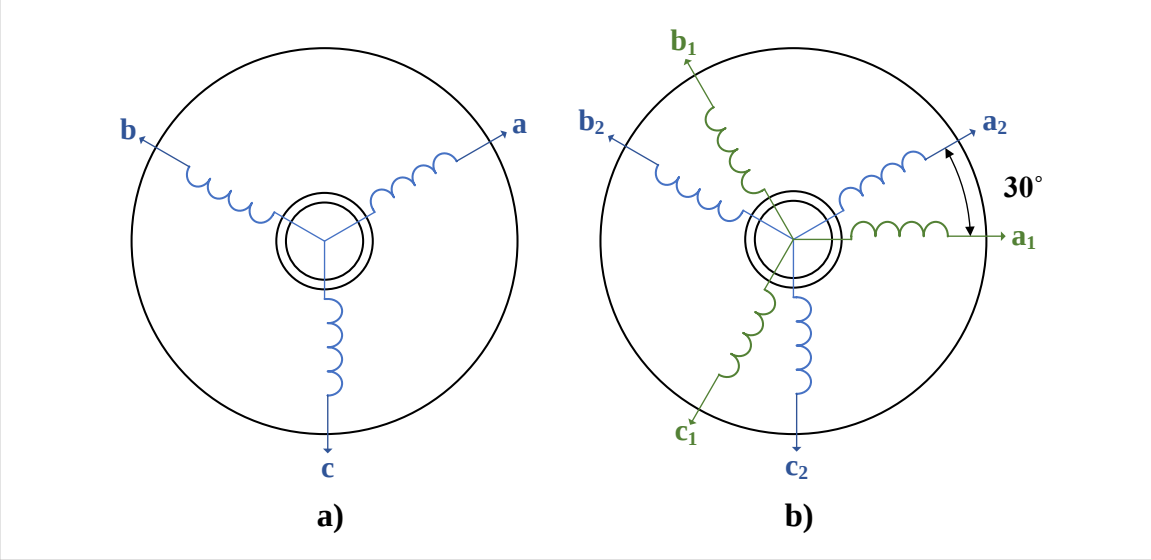

Figure 1.1: Simple representation of a: a) Three phase motor b) dual-three phase motor

In controlling DTP-PMSMs, standard field-oriented control algorithms can be adapted from the control of three phase machines [Hadiouche et al.(2006)Hadiouche, Baghli, and Rezzoug]. They map the currents to a synchronous reference frame and then use PI controllers to command a voltage that moves the currents to the desired reference. However, due to the increased complexity of multi-phase motors, these controllers can experience reduced performance during transients. As such, many researchers are looking into alternative control techniques to deal with this issue.

In recent years, model predictive control is being seen as a solution. [Tenconi et al.(2018)Tenconi, Rubino, and Bojoi]. Model predictive control uses the mathematical model of the system to predict the future system states. It then picks the most optimum state to minimize the error, based off of that prediction. Compared to conventional PI controllers MPC algorithms have an improved dynamic response, can be versatile to non-linearities, and can achieve optimum performance [Schwenzer

et al.(2021)Schwenzer, Ay, Bergs, and Abel, Rodriguez and Cortes(2012)]. To reduce the complexity in finding the optimum state it is common in the literature to use finite-control-set model predictive control (FCS-MPC) [Gonçalves et al.(2019)Gonçalves, Cruz, and Mendes]. This limits the control actions to a limited set of options. In the application of motor control, this control set is all of the possible states of the inverter. However, as this is a relatively new topic of research, there are many problems with the algorithms. FCS-MPC control algorithms suffer from large steady-state ripples, are sensitive to modelling errors, and have a variable switching frequency [Tenconi et al.(2018)Tenconi, Rubino, and Bojoi, Liu et al.(2018-06)Liu, Li, and Zheng].

The goal of this thesis is to introduce three new improvements to the FCS-MPC algorithm applied to dual-three phase PMSMs. Firstly, the mathematical model of the machine is augmented to be based off of flux instead of inductance, which allows for better predictions of the motor states. Then, the incremental model of the machine is used to reduce the steady-state errors of the model. Finally, a dynamic vector search space algorithm is introduced to eliminate the steady-state ripple and make the tracking more precise.

1.2 Contributions

In contribution to this work, articles have been published on this topic. They are listed below:

- Virtual-Flux Finite Control Set Model Predictive Control of Dual-Three Phase IPMSM Drives- [Agnihotri et al.(2021)Agnihotri, Valencia, Taha, and Nahid-Mobarakeh]

- A Review of Model Predictive Control Techniques for Dual-Three Phase Permanent Magnet Synchronous Motors. This paper is currently under review to be published in IEEE Access.

1.3 Thesis Outline

The rest of this thesis can be organized as follows:

- The second chapter shows the literature review about the topic, from developing the model of the DTP-PMSM, to developing the model-predictive control algorithm for DTP-PMSMs.
- The third chapter introduces the development of the virtual flux, incremental model, and dynamic vector search space.
- The fourth chapter describes the implementation of the algorithm on an experimental setup. The results of the experiments are then presented.
- Finally, the sixth chapter concludes the work and introduces future work to further improve the algorithm

Chapter 2

State of the Art: Dual-Three Phase Drives and Model Predictive Control

The main goal of this thesis is to develop a current controller of a dual-three phase motor using model-predictive control. MPC algorithms are simple, however, to effectively implement them it is important to understand how they function. The same can be said about dual-three phase machines. The principles of the control of DTP PMSMs are adapted from their three phase counterparts, however, one needs to have a understanding of the differences to develop an effective controller.

In this chapter, a literature review of the topics are presented. First, the modelling and control of three-phase motors is discussed. Then these concepts are extended to the modelling and control of dual-three phase PMSMs. Next, the concept of model predictive control is discussed; from the general implementation, to the implementation on DTP-PMSMs. Finally, the strengths and weaknesses of the current methods

are detailed.

2.1 Electric Motors

2.1.1 Brief History of Electric Vehicles

Electric motors are at the centre of of electric vehicles (EVs). They exploit the interactions of magnetic fields to produce a torque. This property has been used for a long time, with examples dating back as early as 1839 [Michalowicz(1948)]. From electric boats to cars, utilizing electricity for movement has been a common goal of inventors. In the early 1900's EV's were as popular as steam and internal combustion engines (ICE), with the majority of vehicles in urban centres being fully electric [Ajanovic(2015)]. However, as the demand for a higher range increased, coupled with the mass production of internal combustion engines, the demand for electric cars quickly decreased. Between 1930-1970 they virtually disappeared from the market. In modern times, due to the global climate crisis, as well as the improved technology, electric vehicles are becoming more popular, with many large automotive manufacturers selling hybrids and EVs [Ewing(2022)].

2.1.2 Permanent Magnet Synchronous Motors

As mentioned in section 1, Permanent magnet synchronous motors are a popular in EVs. They have strong permanent magnets mounted on the rotor, with coils on the stator. A simple representation can be seen in Fig. 2.1. When an electric current is passed through the stator, it produces a magnetic field, which interacts with the field from the magnets, thereby producing a torque. Compared to other motor types,

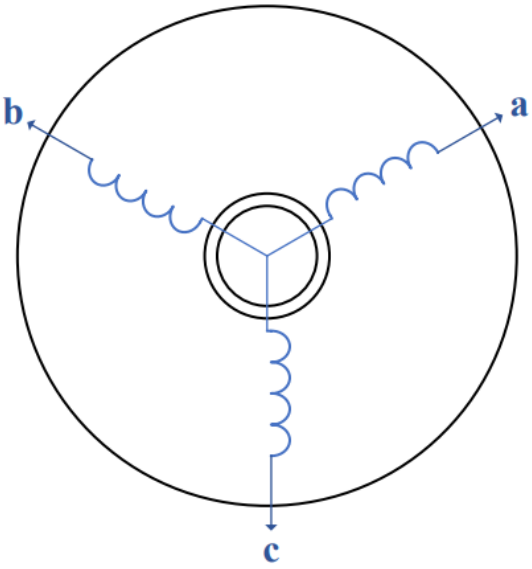

Figure 2.1: Simple ideal Circuit representation of a three phase PMSM

they have a higher efficiency as well as torque density. [Hashemnia and Asaei(2008)]. Therefore, a smaller sized motor can be used to get the same power output, compared to other motor types. There are two types of PMSMs that are generally used:

- *Surface Mounted Permanent Magnet Synchronous Motors (SPMSM)* - with the magnets mounted on the surface of the rotor.
- *Interior Permanent Magnet Synchronous Motors (IPMSM)* - with the magnets embedded into the rotor.

The two different motors can be seen in Fig 2.2. The parameter affected by the mounting methods is the magnetic saliency. On an IPMSM, the magnets are embedded into the rotor, this makes the magnetic flux-linkage asymmetrical. However, on an SPMSM the magnets are mounted on the surface so follow the curve of the rotor. As such, the magnetic field is symmetrical withing the air gap. A salient magnetic

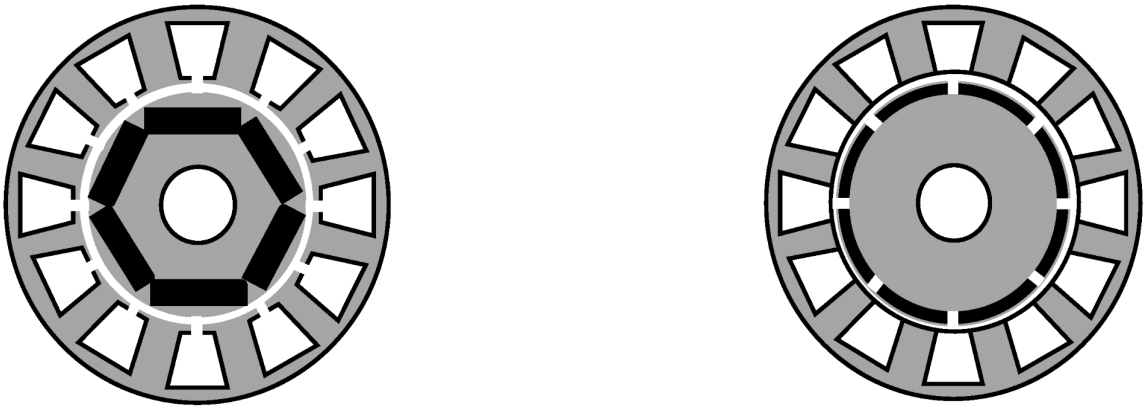

Figure 2.2: Simple diagram of the structure of a: a) Interior Permanent Magnet Synchronous Motor b) Surface Mounted Permanent Magnet Synchronous Motor [Liu et al.(2020)Liu, Tu, Lin, and Liu]

field means that one can utilize both interaction torque and reluctance torque [Murakami et al.(1999)Murakami, Honda, Kiriyama, Morimoto, and Takeda], albeit at the cost of more complex control. This allows for a higher torque to be produced with a lower current, which is why IPMSM's are generally preferred in applications where efficiency is key.

2.2 Field Oriented Control of PMSM Drives

The main output of any motor is the torque. The torque produces angular acceleration, which is used to move the rotor. As stated before, in an electric motor the torque results from the interactions of the magnetic fields on the stator and rotor. To produce rotation from the rotor, one must produce a rotating magnetic field around it. To produce this rotating magnetic field, one controls the applied voltage into the coils, which in turn induces a current, which in turn, creates a magnetic flux-linkage.

The best method of control for PMSMs is by field oriented control, which will be described in the following subsections. The majority of this section was taken from course materials from "ECE788 Adjustable Speed Drives" [Nahid-Mobarakeh(2020)].

2.2.1 Modelling of Three-phase PMSMs

The simple model of PMSM can be represented by a magnet rotating at the centre of three coils. For a three phase motor wired in the Y-configuration, the equivalent circuit equation can be represented by:

$$v_p = R_s \cdot i_p + \frac{d}{dt}\psi_p \tag{2.1}$$

Where v_p represents the phase to neutral voltage across the coil, R_s the resistance, and ψ_p the flux linkage passing through the coil.

For a three-phase machine, this equation can be made for each of the phases *abc*. Therefore, for a three-phase PMSM, the flux-linkage equations become:

$$\begin{bmatrix} v_a \\ v_b \\ v_c \end{bmatrix} = R_s \begin{bmatrix} i_a \\ i_b \\ i_c \end{bmatrix} + \frac{d}{dt} \begin{bmatrix} \psi_a \\ \psi_b \\ \psi_c \end{bmatrix} \tag{2.2}$$

Furthermore, if the neutral point of the motor is isolated, then the following equation holds:

$$i_a + i_b + i_c = 0 \tag{2.3}$$

Which, means that there are only two independent currents that need to be controlled. Therefore, one can use a transformation to turn the subspace from one based on three variables to two. The two transformations that accomplish this are: the Clarke transformation and the Concordia transformation. The two transformations achieve a similar result, however, the Clarke transformation is current and voltage invariant while the Concordia transformation is power invariant. This means depending on the transformation used, either the voltage/current or power will have the same magnitude. For this paper the Clarke transform was used, and this thesis will only discuss the equations based on it. The transformation matrix can be seen in the following equation:

$$\begin{bmatrix} x_a \\ x_b \\ x_c \end{bmatrix} = \begin{bmatrix} 1 & 0 \\ \frac{-1}{2} & \frac{\sqrt{3}}{2} \\ \frac{-1}{2} & \frac{-\sqrt{3}}{2} \end{bmatrix} \cdot \begin{bmatrix} x_\alpha \\ x_\beta \end{bmatrix} \tag{2.4a}$$

$$\begin{bmatrix} x_\alpha \\ x_\beta \end{bmatrix} = \frac{2}{3} \cdot \begin{bmatrix} 1 & \frac{-1}{2} & \frac{-1}{2} \\ 0 & \frac{\sqrt{3}}{2} & \frac{-\sqrt{3}}{2} \end{bmatrix} \cdot \begin{bmatrix} x_a \\ x_b \\ x_c \end{bmatrix} \tag{2.4b}$$

The result of this transform gives a space vector with two components; one called the α component and one called the β, which are 90 degrees with respect to each other. To produce the rotating magnetic field, one would have sine-wave references for the α and β currents. However, when used in this way the tracking of the optimal α and β voltages can be difficult since they depend on the rotor position. Therefore, the park transform is usually applied in conjunction with the Clarke transformation.

This shifts the reference frame to be in line with the position that generates the most torque. Usually, the transforms are applied so that the current at phase a is at a positive maximum. As a result of this, to control the torque of the machine, one only needs to track a constant reference as opposed to an alternating one. The formula for the park transformation as well as the inverse can be seen in Eq. 2.5a seen below:

$$\begin{bmatrix} x_\alpha \\ x_\beta \end{bmatrix} = \begin{bmatrix} cos\theta & -sin\theta \\ sin\theta & cos\theta \end{bmatrix} \cdot \begin{bmatrix} x_d \\ x_q \end{bmatrix} \tag{2.5a}$$

$$\begin{bmatrix} x_d \\ x_q \end{bmatrix} = \begin{bmatrix} cos\theta & sin\theta \\ -sin\theta & cos\theta \end{bmatrix} \cdot \begin{bmatrix} x_\alpha \\ x_\beta \end{bmatrix} \tag{2.5b}$$

This transforms the α and β components into d (direct) and q (quadrature) components, with the d components being in line with the permanent magnets. This requires accurate knowledge of the rotor position, which usually requires the use of an extra sensor. As a result of the Park transformation, to get the parameters of the machine in terms of the transformations one can apply the Clarke and Park transformation to the circuit model presented in Eq. 2.1. The motor model in the dq-reference frame becomes:

$$\begin{bmatrix} v_d \\ v_q \end{bmatrix} = R_s \cdot \begin{bmatrix} i_d \\ i_q \end{bmatrix} + \frac{d}{dt} \begin{bmatrix} \psi_d \\ \psi_q \end{bmatrix} + \omega \cdot \begin{bmatrix} 0 & -1 \\ 1 & 0 \end{bmatrix} \cdot \begin{bmatrix} \psi_d \\ \psi_q \end{bmatrix} \tag{2.6}$$

Where ω is the electrical frequency of the machine. In the conventional control of three-phase PMSMs, the last change to the model comes from the flux-linkages. It is not easy to directly measure the flux-linkages of the machine directly, therefore, they

are usually referenced in terms of their inductance's and currents as seen in formulas below:

$$\psi_d = L_d \cdot i_d + \psi_f \tag{2.7a}$$

$$\psi_q = L_q \cdot i_q \tag{2.7b}$$

Where ψ_f represents the flux-linkage constant from the permanent magnets. This model is all that is needed to design the controller. However, it is only valid under certain assumptions:

- Three phases are balanced
- Distribution of magneto-motive forces is sinusoidal
- Magnetic circuit is not saturated
- Damping effect at rotor is neglected
- Air gap irregularities are ignored
- Permanent-magnet flux linkage is constant

2.2.2 Control of Three-Phase Drives

The block diagram for a conventional PI current controller for a PMSM can be seen in Fig. 2.3. The i_{abc} currents and rotor position of the machine are measured and fed into the Clark and Park transformation to obtain i_{dq}. Then those currents along with the reference currents go into proportional integral controllers, which output reference voltage. Finally the reference voltages fed into a modulator, which uses a

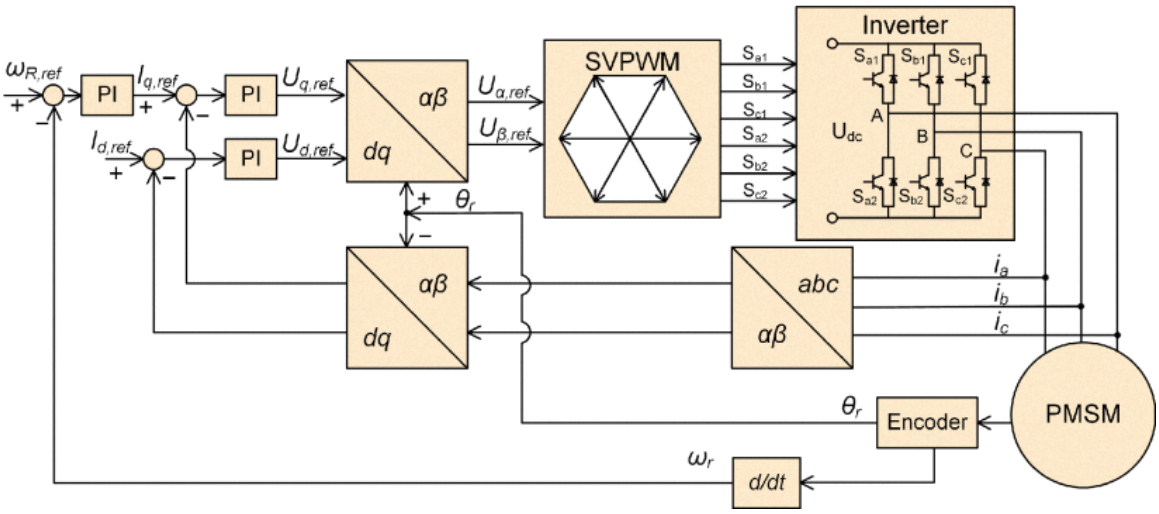

Figure 2.3: Block diagram of a conventional PI FOC current controller. From [Liu et al.(2020)Liu, Tu, Lin, and Liu], as part of the Creative Commons License

switching patterns to generate the desired reference voltage. If one wishes to control the speed of the PMSM, a separate outer loop that controls the q current can be used, however, the design of this loop is beyond the scope of this paper.

2.2.3 Proportional Integral Current Control

Proportional integral control is a simple but effective way to track the reference currents of the motor. With this technique, the error and the integral of the error are multiplied by a scaling value. The output of which is the control action that reduces the error to zero. The proportional term determines how fast the controller responds while the integral term eliminates the steady state error.

The design process for such a controller will be discussed for the d current, however, the exact same process can be used for the q current. Furthermore, the same process can be extended for dual-three phase PMSMs as well. The method that will be described is the pole-zero compensation method. The following equation is the

transfer function of a PI controller in the s domain:

$$C_d(s) = K_{pd} \cdot \frac{\tau_{id} \cdot s + 1}{\tau_{id} \cdot s} \tag{2.8}$$

where,$\tau_{id} = \frac{K_{pd}}{K_{id}}$ and the following equation is the transfer function of the machine d current, based off of the circuit model:

$$G_d(s) = \frac{1}{R_s} \cdot \frac{1}{\tau \cdot s + 1} \tag{2.9}$$

where $\tau = \frac{L_d}{R_s}$. By choosing the numerator of the controller transfer function to be the same as the d current transfer function, the pole from the i_d current is eliminated. This turns the closed loop transfer function to:

$$T(s) = \frac{1}{\frac{L_d}{K_{pd}} \cdot s + 1} \tag{2.10}$$

The time constant is represented by $\frac{L_d}{K_{pd}}$, so one can determine the response time by choosing the K_{pd}. After that, one can calculated the integral gain $K_{id} = \frac{K_{pd}}{\tau_{id}}$.

After the reference voltage has been determined by the PI controllers it is necessary to account for the for the non-linearity caused by the motor speed. As seen in Eq. 2.6, there is exists a cross coupling terms between the the two axis. This cross coupling can cause the two terms to affect each other; when one reference changes, the other one is affected as well. To compensate for this, one can subtract the cross coupling terms out of the PI voltages. This can be seen in Fig. 2.4.

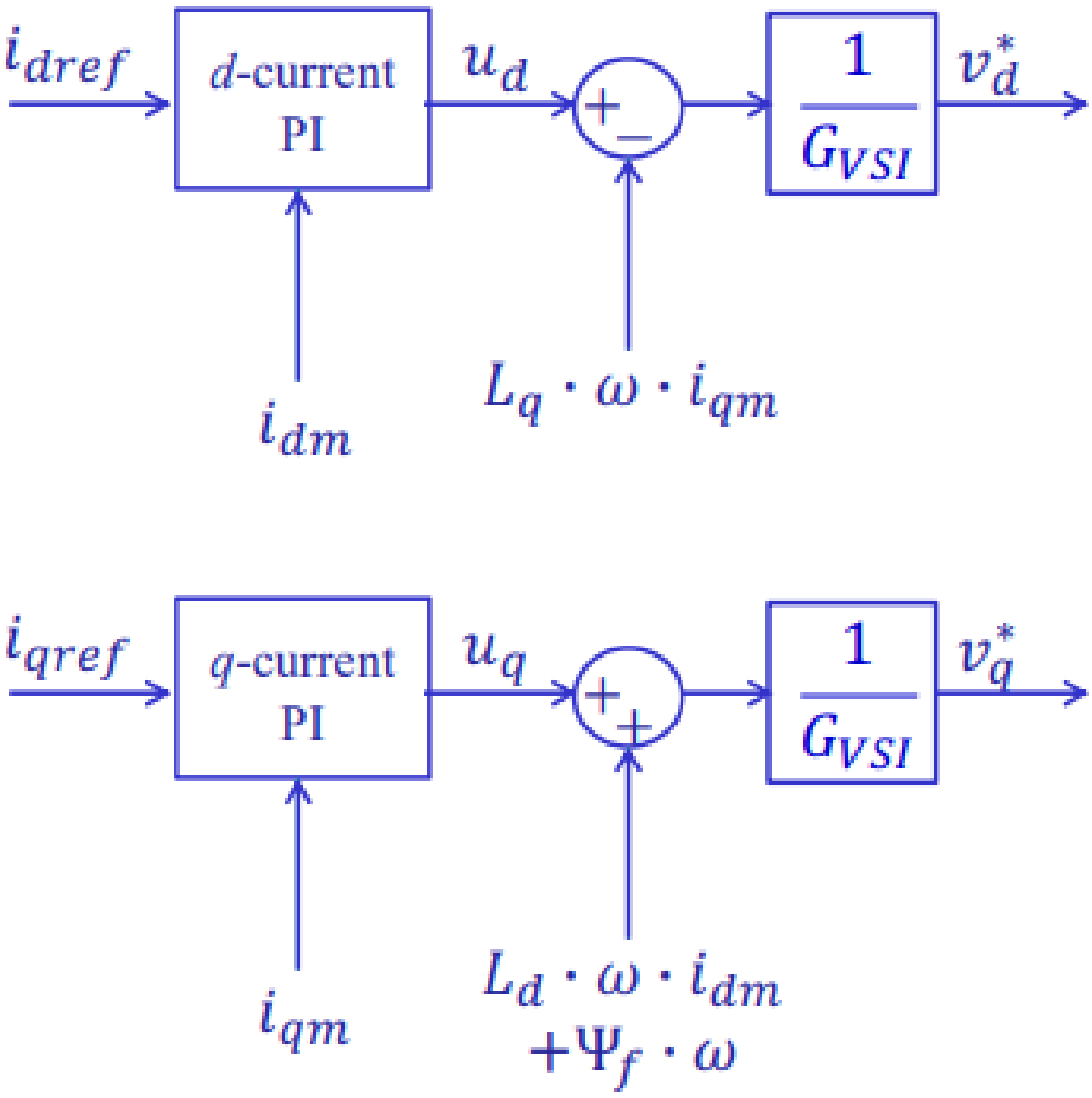

Figure 2.4: Block Diagram of a PI current controller controller for a three phase machine. Taken from [Nahid-Mobarakeh(2020)]

2.2.4 Modulation

To generate the voltage references from the controller, one requires a voltage source inverter, which can generate the AC voltage waveform using modulation. For a three-phase PMSM, a two-level voltage source inverter is usually used. A simplified circuit diagram can be seen in Fig. 2.5. A two level VSI for a three phase machine consists of three legs with six switches. In a leg, when the top switch is turned on while the bottom switch is off, the output voltage is brought to the DC-link voltage. When the bottom switch is turned on while the top switch is off, the voltage is brought to ground. These are the two options that the switches are used in. The two switches in a leg should not be turned on at the same time as this produces a short to ground.

To generate the voltage reference from the VSI, two modulation methods are mainly used: sinusoidal modulation and space vector modulation. Sinusoidal modulation compares the reference voltage to a triangular carrier wave; when the carrier wave is smaller than the reference, the voltage is turned on, and vice versa. A diagram of this can be seen in Fig. 2.6.

Sinusoidal modulation is easy to implement, however, it generally has a poor DC bus utilization. The maximum phase-phase voltage that can be produced without going into over-modulation is $0.612V_{DC}$. Over-modulation results in a larger THD so it is best to avoid operating in that region under normal conditions.

To account for this shortcoming a better method of modulation is space vector modulation. The maximum phase voltage able to be produced without over-modulation for this technique is $0.744V_d$. To generate the reference voltages, space vectors based off the Clarke transformation are used. A two-level VSI has 8 different combinations it can be turned on in. Six of these combinations produce unique space

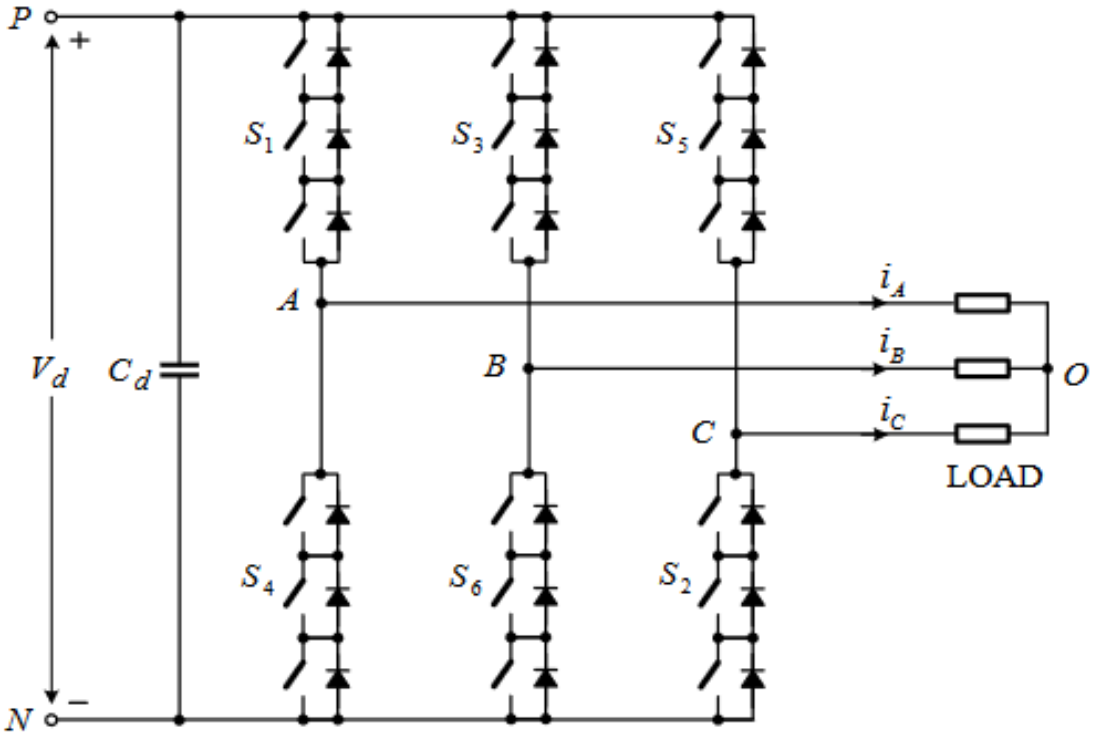

Figure 2.5: Simple schematic representation of a three phase two-level inverter. From [Narimani(2021)]

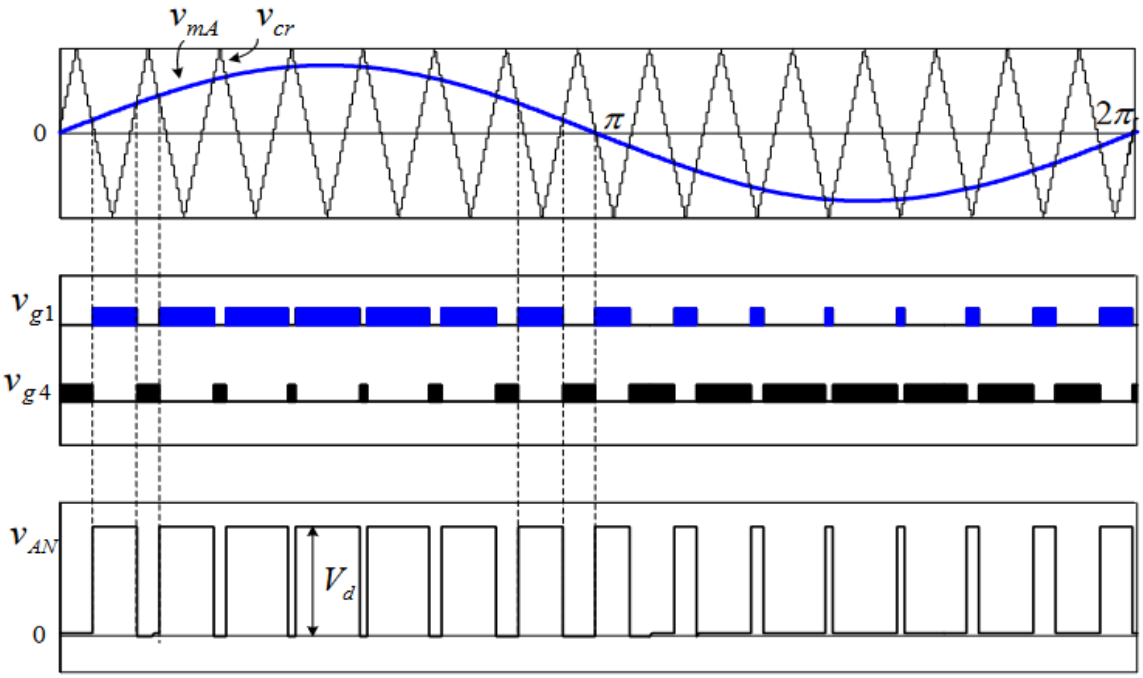

Figure 2.6: Example of modulating waveform and reference waveform used for sinusoidal modulation. From [Narimani(2021)]

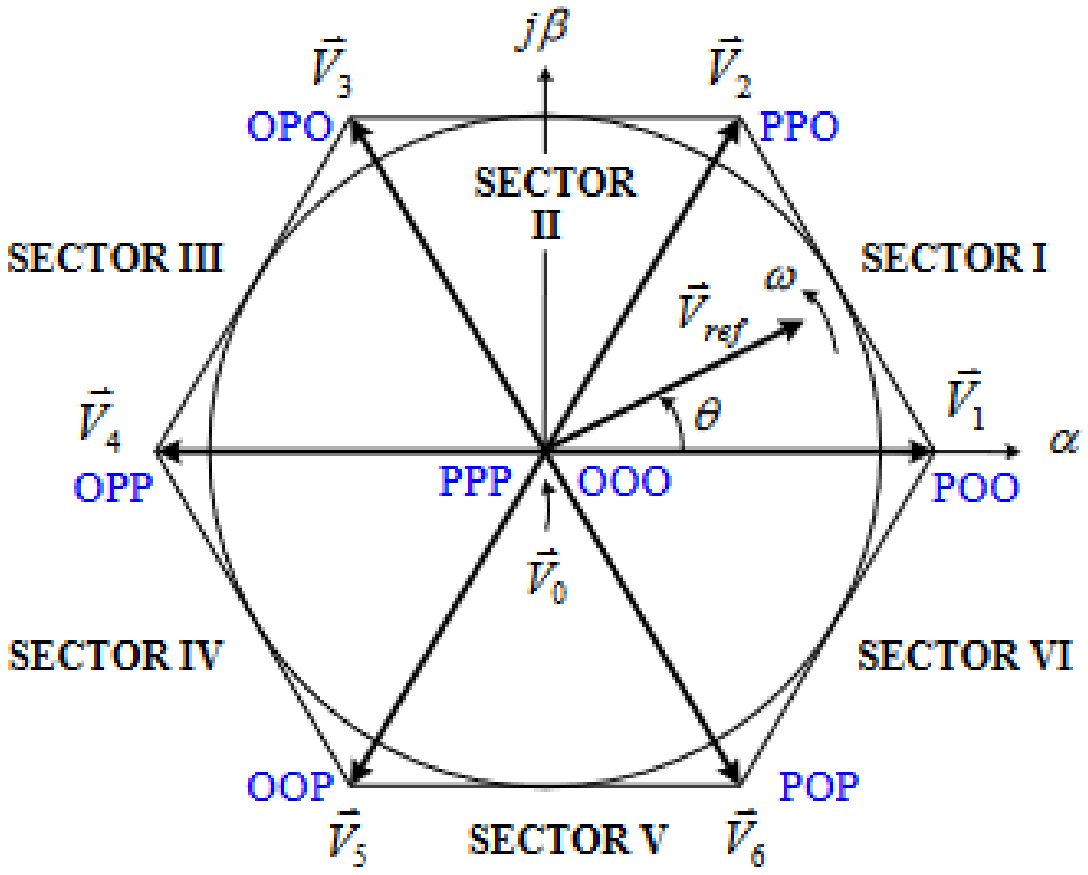

Figure 2.7: Diagram of the Space Vector Modulation Vectors and Sectors for a three phase inverter. Taken from [Narimani(2021)]

vectors, with the other two being zero vectors. The main concept of space vector modulation is to generate a precise new vector from the combination of two active vectors. From the five active space vectors one only needs to choose two to generate the new vector. The two vectors closest to the reference one are chosen, which separates the space into five sectors. The sectors referenced can be seen in Fig. 2.7. The formulas for the duty cycles of the vectors are:

$$T_a = \frac{\sqrt{3}T_s V_{ref}}{V_d} \cdot sin(\frac{\pi}{3} - \theta) \tag{2.11a}$$

$$T_b = \frac{\sqrt{3}T_s V_{ref}}{V_d} \cdot sin(\theta) \tag{2.11b}$$

$$T_0 = T_s - T_a - T_b \tag{2.11c}$$

where T_a is the duty cycle of the top vector, T_b is the duty cycle of the bottom vector, and T_0 is the duty cycle of the zero vector. However, to ensure a constant switching frequency as well as as a reduced THD, it is necessary to apply the vectors in such a way that each leg is only applied once during a switching period. One can create such a pattern using 7 segments. An example seven-segment switching pattern can be seen in Fig. 2.8. With each sector the order that the vectors being applied is changed, but the general concept remains the same.

2.2.5 Dual-Three Phase PMSMs and Current Control

A simplified diagram of an asymmetrical dual-three phase machine can be seen in Fig. 2.9. When developing a controller for such a machine the same approach can be taken as the one discussed in section 2.2.2. The same concepts of field-oriented control

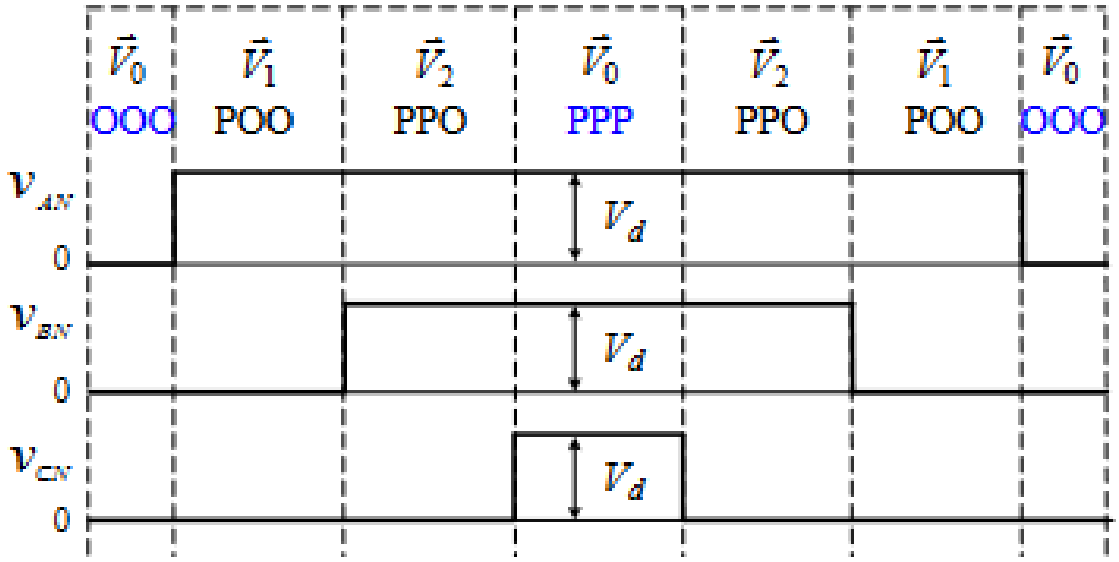

Figure 2.8: Diagram of a Seven Segment Switching Sequence for three phase space vector modulation. Taken from [Narimani(2021)]

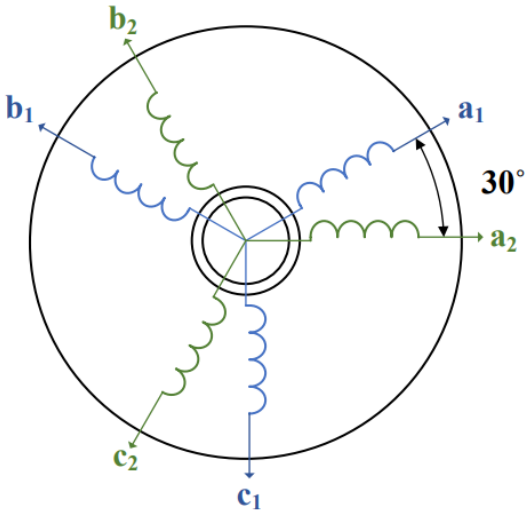

Figure 2.9: Simplified ideal circuit representation of a Dual-three phase PMSM

apply, however, the extra phases introduce extra variables that need to be accounted for. Instead of there being two independent currents that need to be controlled there are four; two for each three-phase winding set. A simple transformation that can be used is the double dq transformation, which is essentially the Clarke transformation, applied to each of the winding sets individually. The transformation matrix can be seen below:

$$\begin{bmatrix} \alpha_1 \\ \beta_1 \\ \alpha_2 \\ \beta_2 \\ 0 \\ 0 \end{bmatrix} = \begin{bmatrix} 1 & -\frac{1}{2} & -\frac{1}{2} & 0 & 0 & 0 \\ 0 & \frac{\sqrt{3}}{2} & -\frac{\sqrt{3}}{2} & 0 & 0 & 0 \\ 0 & 0 & 0 & \frac{\sqrt{3}}{2} & -\frac{\sqrt{3}}{2} & 0 \\ 0 & 0 & 0 & \frac{1}{2} & \frac{1}{2} & -1 \\ \frac{1}{3} & \frac{1}{3} & \frac{1}{3} & 0 & 0 & 0 \\ 0 & 0 & 0 & \frac{1}{3} & \frac{1}{3} & \frac{1}{3} \end{bmatrix} \begin{bmatrix} a_1 \\ b_1 \\ c_1 \\ a_2 \\ b_2 \\ c_2 \end{bmatrix} \tag{2.12}$$

However, as proposed by Zhao and Lipo [Zhao and Lipo(1995)], this transformation may not utilize the full potential of DTP-PMSMs. By creating a transformation that separates the harmonics into orthogonal sub-spaces, one can have better control over the overall THD. As per the VSD transformation the fundamental and $k = 12m \pm (m = 1, 2, 3, ...)$ torque producing components are mapped to the dq frame, the fifth and seventh $k = 6m \pm 1, (m = 1, 3, 5, ...)$ are mapped to another subspace called the xy plane, and the zero order harmonics are mapped to the third subspace. If the neutral points are isolated, then the zero-sequence components can be disregarded. The transformation matrix technique can be seen in the following equation:

$$\begin{bmatrix} \alpha \\ \beta \\ x \\ y \\ 0 \\ 0 \end{bmatrix} = \begin{bmatrix} 1 & -\frac{1}{2} & -\frac{1}{2} & \frac{\sqrt{3}}{2} & -\frac{\sqrt{3}}{2} & 0 \\ 0 & \frac{\sqrt{3}}{2} & -\frac{\sqrt{3}}{2} & \frac{1}{2} & \frac{1}{2} & -1 \\ 1 & -\frac{1}{2} & -\frac{1}{2} & -\frac{\sqrt{3}}{2} & \frac{\sqrt{3}}{2} & 0 \\ 0 & -\frac{\sqrt{3}}{2} & \frac{\sqrt{3}}{2} & \frac{1}{2} & \frac{1}{2} & -1 \\ 1 & 1 & 1 & 0 & 0 & 0 \\ 0 & 0 & 0 & 1 & 1 & 1 \end{bmatrix} \begin{bmatrix} a_1 \\ b_1 \\ c_1 \\ a_2 \\ b_2 \\ c_2 \end{bmatrix} \tag{2.13}$$

From these transforms the park transformation is also applied. For the park transformation, one can either keep the xy currents in the stationary reference frame, the positive synchronous reference frame, or the negative synchronous reference frame. Using the xy currents in the negative reference frame allows for easier injection of xy currents to account for the unbalances of the machine [Hu et al.(2014)Hu, Zhu, and Liu, Duran et al.(2017)Duran, Gonzalez-Prieto, Barrero, Levi, Zarri, and Mengoni]. The transformation can be seen below:

$$\mathbf{T_{rot}}(\theta_e) = \begin{bmatrix} \mathbf{T_{park}}(\theta_e) & \mathbf{0}_{2\times2} & \mathbf{0}_{2\times2} \\ \mathbf{0}_{2\times2} & \mathbf{T_{park}}(-\theta_e) & \mathbf{0}_{2\times2} \\ \mathbf{0}_{2\times2} & \mathbf{0}_{2\times2} & \mathbf{I}_{2\times2} \end{bmatrix}, \tag{2.14a}$$

Similar to the model developed for three-phase machines, the dual-three phase machine model becomes:

$$\begin{bmatrix} u_d \\ u_q \\ u_x \\ u_y \\ u_{z1} \\ u_{z2} \end{bmatrix} = R_s \begin{bmatrix} i_d \\ i_q \\ i_x \\ i_y \\ i_z1 \\ i_z2 \end{bmatrix} + \frac{d}{dt} \begin{bmatrix} \psi_d \\ \psi_q \\ \psi_x \\ \psi_y \\ \psi_{z1} \\ \psi_{z2} \end{bmatrix} + \omega_e \begin{bmatrix} 0 & -1 & 0 & 0 & 0 & 0 \\ 1 & 0 & 0 & 0 & 0 & 0 \\ 0 & 0 & 0 & 1 & 0 & 0 \\ 0 & 0 & -1 & 0 & 0 & 0 \\ 0 & 0 & 0 & 0 & 0 & 0 \\ 0 & 0 & 0 & 0 & 0 & 0 \end{bmatrix} \begin{bmatrix} \psi_d \\ \psi_q \\ \psi_x \\ \psi_y \\ \psi_{z1} \\ \psi_{z2} \end{bmatrix} \tag{2.15}$$

Where the flux-linkages can be replaced by:

$$\begin{bmatrix} \psi_d \\ \psi_q \\ \psi_x \\ \psi_y \\ \psi_{z1} \\ \psi_{z2} \end{bmatrix} = \begin{bmatrix} L_d & 0 & 0 & 0 & 0 & 0 \\ 0 & L_q & 0 & 0 & 0 & 0 \\ 0 & 0 & L_x & 0 & 0 & 0 \\ 0 & 0 & 0 & L_y & 0 & 0 \\ 0 & 0 & 0 & 0 & L_{z1} & 0 \\ 0 & 0 & 0 & 0 & 0 & L_{z2} \end{bmatrix} \begin{bmatrix} i_d \\ i_q \\ i_x \\ i_y \\ i_z1 \\ i_z2 \end{bmatrix} + \begin{bmatrix} \psi_f \\ 0 \\ 0 \\ 0 \\ 0 \\ 0 \end{bmatrix} \tag{2.16}$$

For creating the current controllers one can use the same process for each of the variables as the one developed in section 2.2.3. However, one needs to add two PI controllers for the xy currents. The block diagram for the controller can be seen in Fig. 2.10. The method of pole-zero compensation is the same for each controller.

For the modulation, the approach that is used is using the double dq transformation to separate the alpha and beta components of each winding set and then using space vector modulation on each set.

This includes the section discussing the design of conventional PI controllers for a

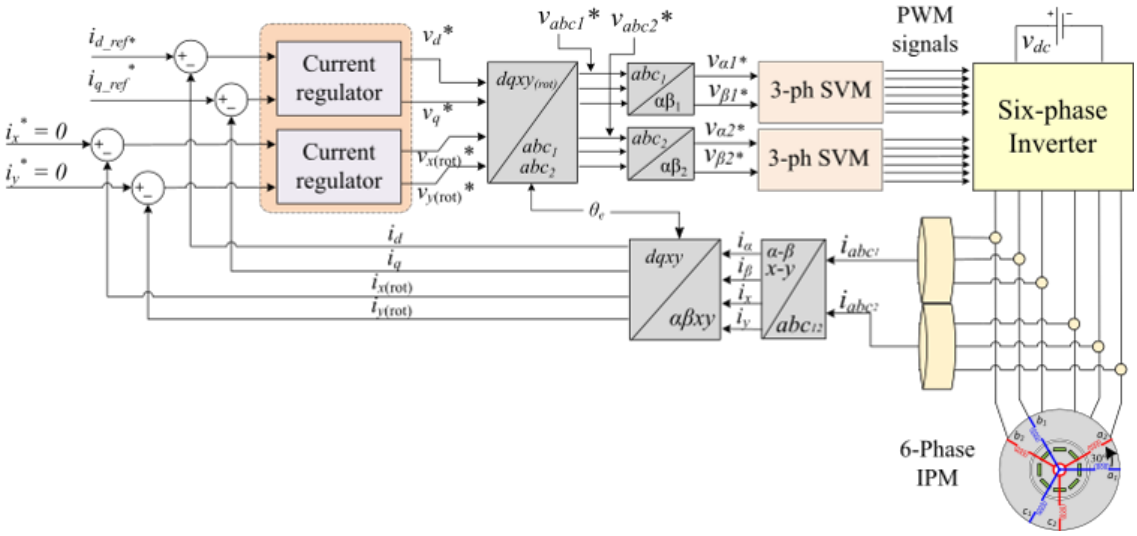

Figure 2.10: Block diagram of a PI-FOC Current Controller for DTP-PMSMs

three-phase as well as dual-three phase machine. The following section introduces the concept of model-predictive control, then details the application to dual-three phase PMSMs.

2.3 Introduction to Model Predictive Control

2.3.1 General State-Space Model

Model predictive control is a widely used technique for many different systems. The concept of the technique is to use the mathematical model to predict the future values of the system, and then to take the control action that minimizes the error–based on the prediction. A simplified block diagram can be seen in Fig. 2.11.

The first step in creating the technique is to understand how one can predict the future states of the model. This is done by discretizing the derivative of the system using a first order Euler-Approximation. This splits the derivative into a future state

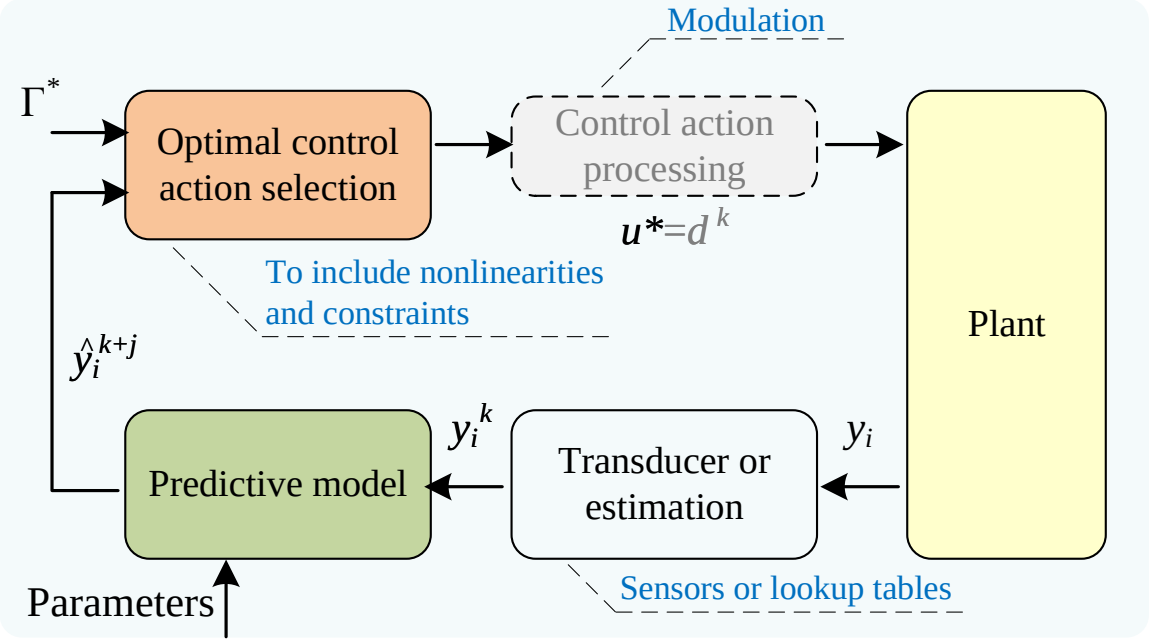

Figure 2.11: General MPC Structure

and a past state. Therefore, to predict the future values of the system one needs to algebraically solve for the future state. However, this is under the assumption that the sampling period is small enough such that there is a small difference between each successive states. To illustrate this technique it can be applied to circuit model of the motor winding in the flux domain. This can be seen in Eq. 2.1:

$$v_p(k) = R_s \cdot i_p(k) + \frac{\psi_p(k+1) - \psi_p(k)}{T_s} \tag{2.17}$$

Where T_s represents the sampling period. It should be noted that k represents 1 sampling period. In other words $x^k = x(kT_s)$. Then solving for the future state the equation becomes:

$$\psi_p(k+1) = T_s(v_p - R_s \cdot i_p(k)) + \psi_p(k) \tag{2.18}$$

Furthermore, this concept can be extended and applied to generate state space systems in terms of their A,B,C matrices. As described by [Wang(2009)], for a state-space system, the prediction equation can be represented by:

$$x(k+1) = Ax(k) + Bu(k) \tag{2.19a}$$

$$y = Cx(k) \tag{2.19b}$$

This describes the equations in one time step. If one wants to predict the future states in multiple time steps, the prediction in $k+1$, is subbed back into the equation. If one does this, in general for n times steps into the future the equation becomes:

$$Y = Fx(k) + \phi u(k) \tag{2.20a}$$

$$F = \begin{bmatrix} CA \\ CA^2 \\ CA^3 \\ CA^n \end{bmatrix} \tag{2.20b}$$

$$\phi = \begin{bmatrix} CB & 0 & 0 & ... & 0 \\ CAB & CB & 0 & ... & 0 \\ CA^2B & CAB & CB & ... & 0 \\ CA^{n-1}B & CA^{n-2}B & CA^{n-3}B & ... & CA^{n-n_c}B \end{bmatrix} \tag{2.20c}$$

The number of steps that the model predicts is called the prediction horizon. After the prediction is made, to find the optimal control action that needs to be taken, one

uses a quadratic cost function of the form:

$$J = (Y_{ref} - Y)^T (Y_{ref} - Y) + \overline{R}U \tag{2.21}$$

the first term $(Y_{ref} - Y)^T$ minimizes the error between the desired values and the predicted values while the second term ($\overline{R}U$ uses a weighting matrix limit the size of the input.

It simple to minimize this cost function considering an unconstrained cost function. One needs to find when the derivative of the cost function is zero. However, this doesn't work in practical situations, as the control action is usually limited. In the case of the DTP-PMSM, there is a limited available voltage from the voltage source inverter. As such, in the practical scenario one will need to employ constrained quadratic programming. This can be difficult to implement in real-time operating systems especially when the sampling time is small.

Am important principle to mention is the concept of receding horizon. After the cost function has been solved one obtains the optimal control action for the predicted values at k predictions [Wang(2009)]. However, if the system is highly non-linear or something changes within that time duration, then the control action predicted may not be optimal. Therefore, after the cost function is solved, only the first (or up to k predictions) control action is implemented. Then at each successive iteration, the model and cost function is solved again. This allows the algorithm to account for the dynamic changes in the model. Another way to account for the large calculation times is to only consider a finite set of the control action. This makes finding the solution easier, especially in multi-variable systems. This is called finite-control set model predictive control.

2.3.2 Finite-Control Set Model-Predictive Control

Finite-control set model predictive control only considers a finite number of options in the cost function. This makes determining the optimum value simpler as one only needs to iterate through each value to find the minimum. This is a common technique in power electronics and multi-phase machines. The following section will review the background information of MPC applied to DTP-PMSMs as well as the current trends in literature.

2.4 Current Trends of Model Predictive Control of Dual-Three Phase Drives

This section will detail the literature review specifically about model-predictive control of dual-three phase machines. This section is pulled from the review article created by the author, which is under review in IEEE Access.

First, one can compare the block diagram of PI controller control to the model predictive controller. This can be seen in Fig. 2.12

As seen in Fig. 2.12 b) the predictive model is used to predict the future states of the *dqxy* currents. Then it picks the optimal state out of all of the options of the inverter. For a two-level VSI with six phases. There are 64 possible vectors to choose from with 49 producing unique space vectors. The possible space vectors can be seen in Fig. 2.13. Therefore, in conventional FCS-MPC the cost function chooses the state out of the 64 options that produces the minimum errors in the currents. This will be further described in the rest of the sections of this chapter.

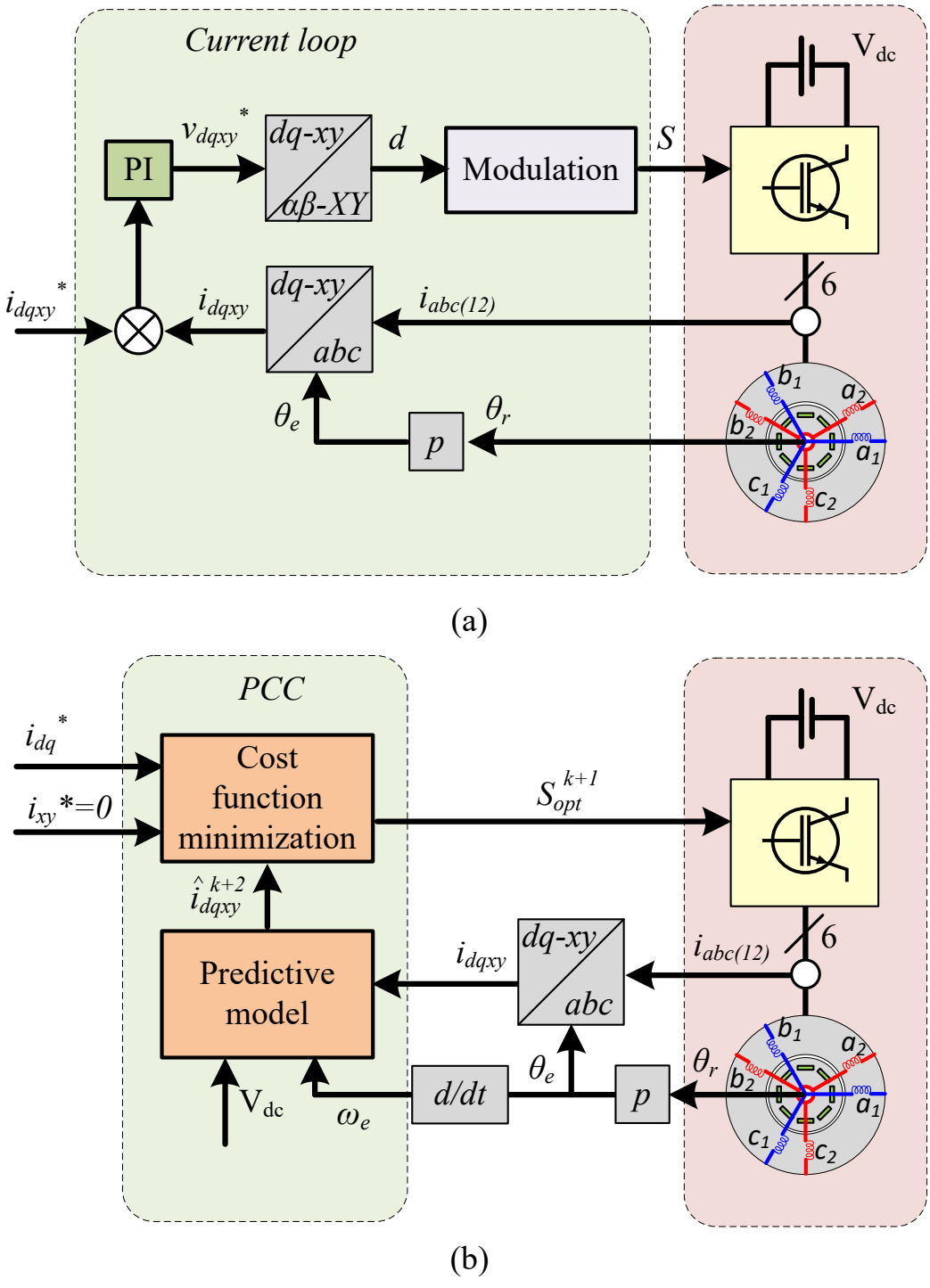

Figure 2.12: Comparison of a a) PI-FOC current controller and b) conventional MPC current controller

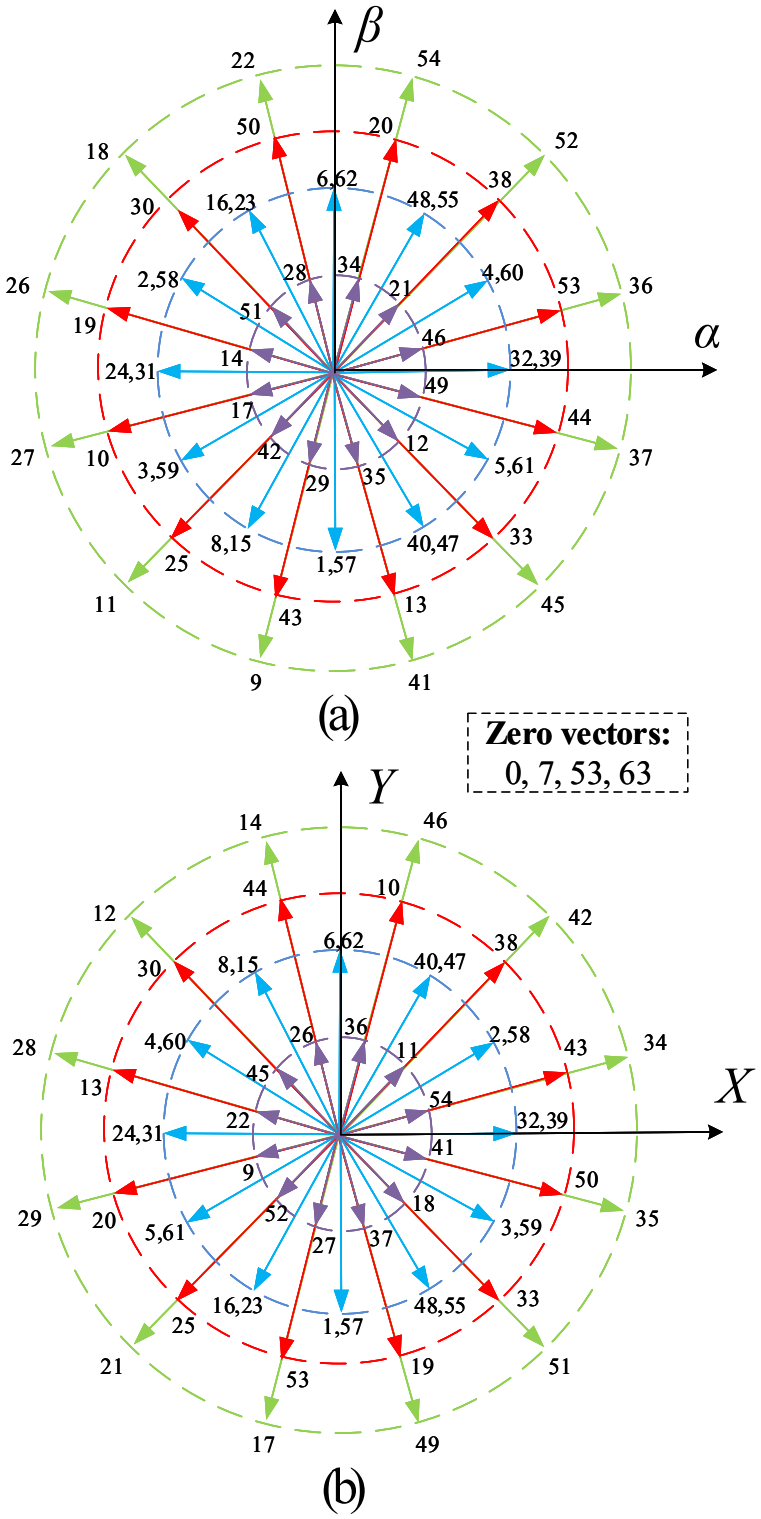

Figure 2.13: a) voltage vectors in α and β subspace b) voltage vectors in X and Y subspace generated for a six-phase two-level inverter

2.4.1 Predictive model

In predictive current control (PCC), the predictive model is intended to estimate or behaviour of the controlled currents at time $k + j$. The simplest approach considers the tracking of the dq reference currents, while minimising the xy components. It is common to define the prediction horizon as $j = 2$ [Cortes et al.(2012)Cortes, Rodriguez, Silva, and Flores]. This two-step horizon compensates for the delay in the measurements, which is known as indirect delay compensation.

One can use many different variations in the predictive model to make the prediction more accurate. The variations can be seen in Fig. 2.14. The accuracy of the model is directly related to the electromagnetic model of the drive and discretization technique. To the best of the author's knowledge, all previous works have adopted the same dynamic model for implementing MPC, based on the VSD transformation. For conventional predictive control, equations 2.15 and 2.16 can be discretized by using the first order Euler approximation. The equation for the future state then becomes:

$$i_d^{k+1} = i_d^k + \frac{T_s}{L_d}\left(v_d^k - R_s i_d^k + \omega_r L_q^k i_q^k\right) \tag{2.22a}$$

$$i_q^{k+1} = i_q^k + \frac{T_s}{L_q}\left[v_q^k - R_s i_q^k - \omega_r \left(L_d^k i_d^k + \psi_{PM}\right)\right] \tag{2.22b}$$

$$i_x^{k+1} = i_x^k + \frac{T_s}{L_x}\left(v_x^k - R_s i_x^k - \omega_r L_y^k i_y^k\right) \tag{2.22c}$$

$$i_y^{k+1} = i_y^k + \frac{T_s}{L_y}\left(v_y^k - R_s i_y^k + \omega_r L_x^k i_x^k\right), \tag{2.22d}$$

where T_s represents the sampling period, and the k the sampling instant. Although

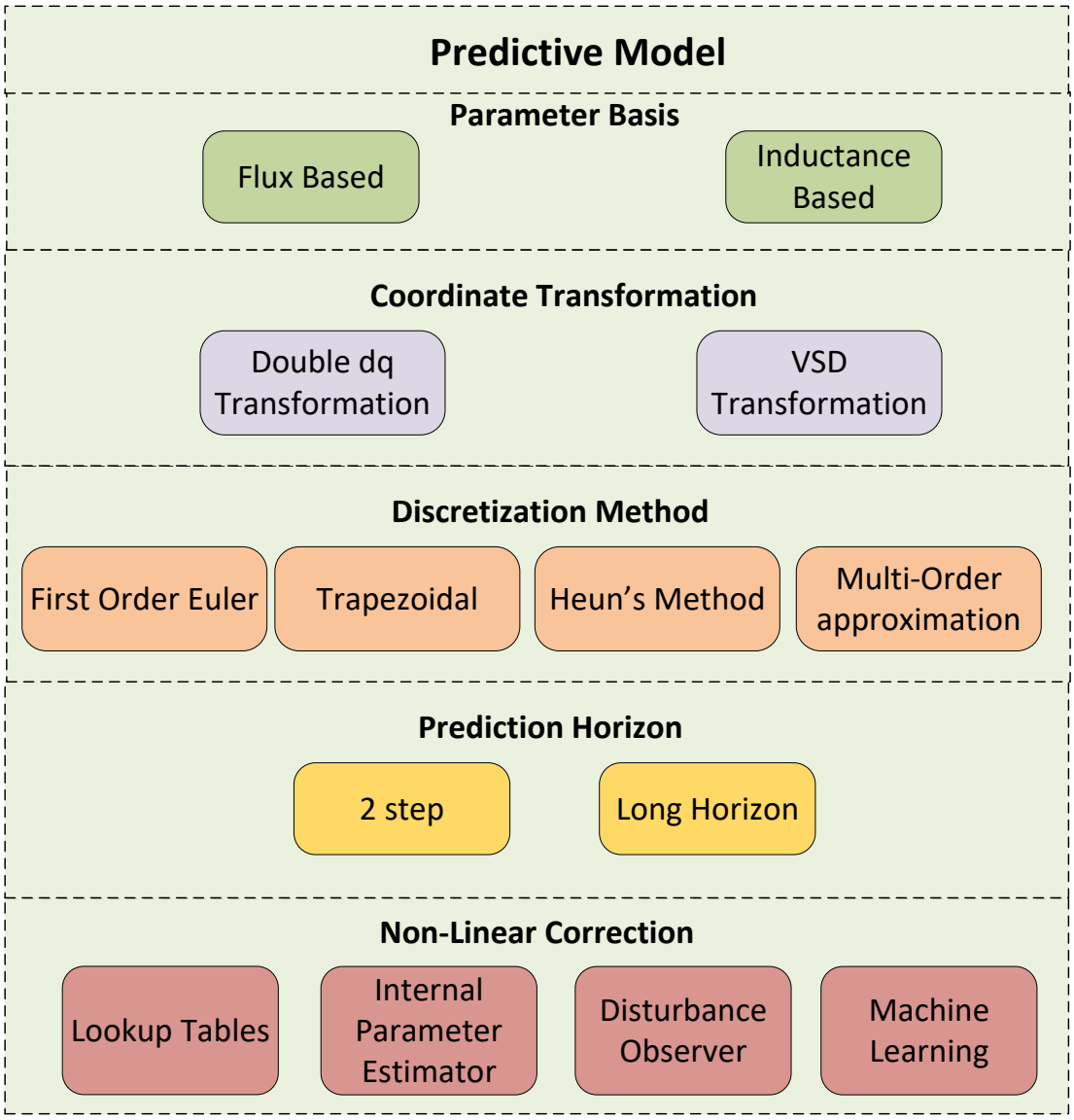

Figure 2.14: Developments that can be made to the predictive model of a PMSM

Euler discretization is the most popular technique, the use of more complex approximation methods can potentially improve the prediction accuracy. Vaclavek and Baha [Vaclavek and Blaha(2013-12)] demonstrated that using Taylor series expansion can improve the performance of the controller at the cost of increasing its complexity. The additional computational cost of using complex models can be handled by the new generation of digital processors [Burkhart et al.(2017)Burkhart, Klein-Hessling, Ralev, Weiss, and Doncker]. However, few studies have been adequately explored in regards to model predictive control of DTP-PMSMs. Recently, the second order trapezoidal rule was used to predict the flux linkages of a DTP-PMSM [Hepp et al.(2020-08)Hepp, Imamovic, Wondrak, and Parspour]. However, although they did show good dynamic and steady-state results, they did not compare the method with the first order approximation, so the actual benefits are yet to be seen.

Regarding the general trends of MPC that can be adapted to DTP-PMSMs, one can look at [Zhang et al.(2018-08)Zhang, Bai, and Yang]. They adapted the model of a three-phase induction motor using a second order discretization method called Heun's method. Furthermore, another paper that showed the advantage of higher order approximation methods was recently published [Khader and Nahla(2021-04)]. They compared the use of the Runge-Kutta approximation method with the conventional Euler approximation for model predictive control of a three-phase inverter. Although they only included simulation results, the results show that using a more accurate prediction model can reduce the output error of the controller.

Although increasing the order of the approximation method can increase the accuracy of the predictive model, one must be wary of increased computational time. Higher order prediction methods require additional calculations to be performed in

the model.

The prediction horizon of MPC is the number of steps in the future predicted by the model. All the studies regarding MPC of DTP-PMSM use a prediction horizon of 2. However, an interesting topic that can be explored in the future for DTP-PMSMs is a longer prediction horizon. This was explained in [Pevec et al.(2019)Pevec, Babic, and Podobnik]. For high-order systems, long-horizon model predictive control can significantly improve the performance of the controller. However, this comes at the expense of higher computational burden. This topic was addressed by P. Karamanakos et al [Karamanakos et al.(2014-03)Karamanakos, Geyer, Oikonomou, Kieferndorf, and Manias], who compared three different strategies to reduce the computational burden of long-horizon model predictive control. This is a popular topic in the current literature. For example, in [Andersson and Thiringer(2020-01)] they proved that for a three-phase electric drive, a prediction horizon of 4 can be implemented in real-time, and produced significantly less switching losses when compared to conventional FOC controllers. Another study used a different approach [Hammoud et al.(2020-10)Hammoud, Hentzelt, Oehlschlaegel, and Kennel], that is, a neural-network based approach to offset the computational burden of a long-horizon MPC applied to a 3-phase IPMSM. The algorithms were tested on an experimental setup as well as in simulation. They found that the neural-network based algorithm was computationally efficient, and had a similar performance when compared to conventional-long horizon FCS-MPC. In general, since the computational burden of MPC has always been an issue, reducing it will always be a major topic in it's research.

A predictive dynamic model allows for a better dynamic response. However, using a model based technique also renders the controller more sensitive to parameter

mismatches [Liu and Liu(2021)]. The flux linkages (and by extension the inductance), vary with parameters such as temperature, rotor position, and current [Taylor et al.(2021)Taylor, Valencia Garcia, Taha, Mohamadian, Luedtke, Nahid-Mobarakeh, Bilgin, and Emadi]. Therefore, using static variables in the predictive model causes increased errors in the current and torque tracking. This issue has been addressed more in the current climate. Liu et al. [Liu and Liu(2021)], used an inductance observer to calculate the real time inductance of the machine. Another solution by Goncalves et al. [Gonçalves et al.(2019)Gonçalves, Cruz, and Mendes], used a disturbance observer to account for the lumped parameter errors associated with the inductance. In other application areas, some researchers have implemented model-free model predictive control, which uses analytical techniques for prediction. This can be exemplified by [Rodríguez et al.(2020)Rodríguez, Heydari, Rafiee, Young, Flores-Bahamonde, and Shahparasti], who implemented a least-squares algorithm to predict the parameters of a voltage source inverter. Because it does not rely on the model of the system, the non-linearities do not affect the prediction as much.In general, reducing the errors of the predictive model will always be of interest because the technique relies heavily on the model.

Regarding the coordinate transformation, the use of the double dq transformation has not been adequately investigated.

2.4.2 Voltage-Vector Search Space

2.4.3 Voltage vector search space

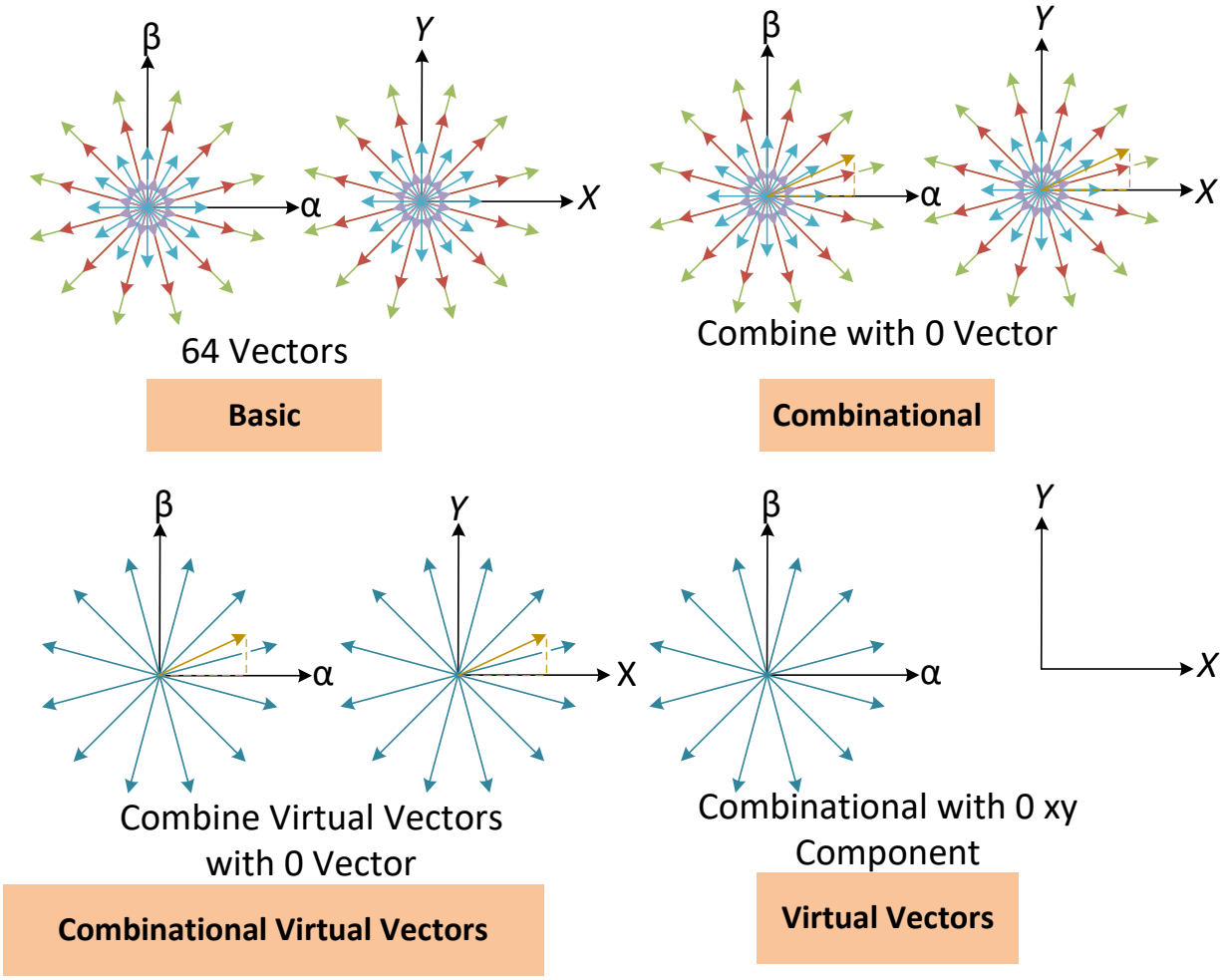

Figure 2.15: Representation of the different vector sub-spaces used in MPC in literature

The voltage vector selection subspace is the focus of most articles on FCS-MPC. There is a large number of choices in what space vectors should be considered in

the algorithm. With a six-phase VSI, there are 64 possible switching states that can be considered, 49 of which provide unique space vectors. This is illustrated in fig 2.13. The number of space vectors in the vector space is directly related to the computational complexity of the algorithm. Therefore reducing that number has been the focus of some researchers. When using conventional FCS-MPC, which uses all 64 vectors, the main issue that arises is the large ripples in the currents [Gonçalves et al.(2019)Gonçalves, Cruz, and Mendes]. Although the optimum state is chosen, because it comes from a discrete set of values, the error can be relatively large.

The first adaptation usually explored is the addition of a zero vector to the switching state. This has been referred to as PWM-FCS-MPC in [Yuan et al.(2020-12)Yuan, Ma, Zhao, and Yang]. This concept is relatively old and is usually used as a comparison to newer techniques that have been developed. The main issue with PWM-FCS-MPC is that it can only change the amplitude of the space vectors and not their direction. Therefore, applying a zero-vector during the sampling period may not reduce tracking errors. This was the main problem addressed by multi-vector MPC [Yuan et al.(2020-12)Yuan, Ma, Zhao, and Yang]. Instead of applying a zero vector in addition to the chosen optimal vector, it selects another vector which may have a different direction and magnitude to bring the error closer to zero. However, since there are four independent variables that need to be controlled–$dqxy$–it can be difficult to obtain a way to get the correct direction and magnitude for all four variables. This problem is primarily addressed by the concept of virtual-vectors. Studies published on virtual-vectors have been the most popular subject regarding predictive current control of DTP-PMSMs. The concept of virtual-vectors is to create a new set of vectors that have a zero magnitude and phase in the xy subspace, but positive in

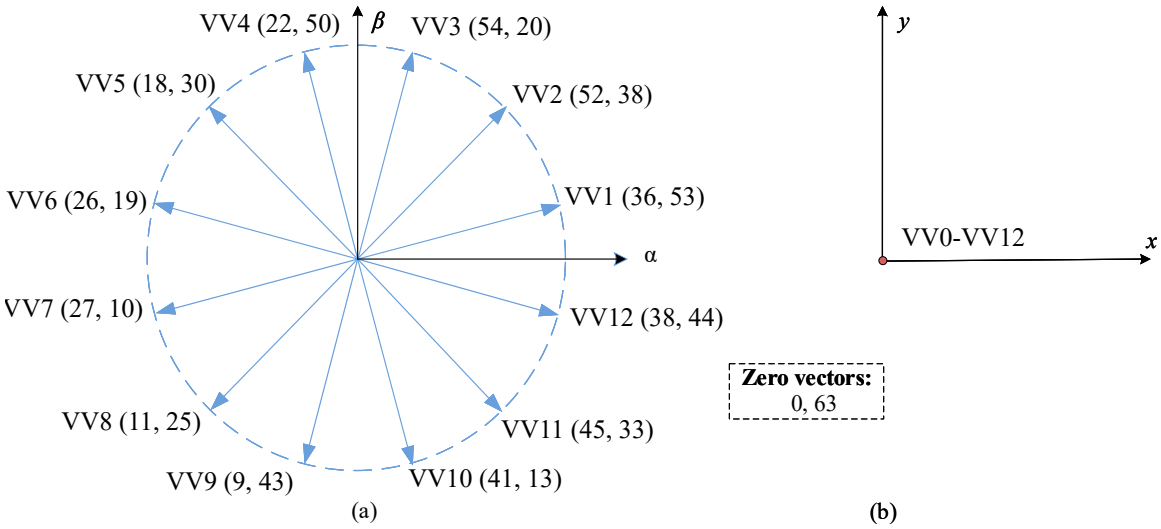

Figure 2.16: Virtual-Vectors based on the VSD transformation in the stationary $\alpha-\beta$, $X-Y$ reference frames

the dq. This can be seen in 2.16. Virtual-vectors are usually created by combining one medium-large vector and a large vector. The resulting combinations have a positive affect in the dq subspace while a zero affect in the xy. As demonstrated by Goncalves et al. [Gonçalves et al.(2019-02a)Gonçalves, Cruz, and Mendes], virtual vector based FCS-MPC controllers generally exhibit the best overall performance. The xy currents are reduced significantly without the additional burden of including variables in the cost function. Further iterations of the technique include variable amplitude virtual-vectors [Gonçalves et al.(2019-02b)Gonçalves, Cruz, and Mendes], which are a combination of a zero vector and virtual-vectors. Another iteration is bi-subspace virtual-vectors, which is a combination of PWM, virtual vector, and multi-vector MPC [Gonçalves et al.(2019)Gonçalves, Cruz, and Mendes]. Regarding the current trends in this area, a prevailing trend is aimed at reducing the vector set size to reduce the number of calculations that need to be performed. This can be seen in the early application of MPC to multi-phase machines in [Duran et al.(2011-08)Duran,

Prieto, Barrero, and Toral], and more recently in [Sahin and Keysan(2018-04)], where they eliminated most of the candidate vectors beforehand. Another trend involves the creation of virtual-vectors using alternative vectors. Recently, Gonzales-Prieto et al. [Gonzalez-Prieto et al.(2022)Gonzalez-Prieto, Martin, González-Prieto, Duran, Carrillo-Ríos, and Aciego] created new virtual-vectors which were a combination of four large vectors to increase voltage utilization. Because this new set had increased rippled in the alpha and beta currents, they only used them in the over-modulation region where higher voltages are required. The development of the voltage vector search space in literature is shown in Fig. 2.15.

2.4.4 Cost-Function

subsectionCost function The cost function selects the optimum state of the VSI. For all algorithms in the literature, the cost function is the error between the reference currents and predicted currents. The cost function in conventional FCS-MPC is,

$$g_i = g_{dq} + \lambda_{xy} \cdot g_{xy} \tag{2.23a}$$

$$g_{dq} = (i_d^* - i_d^{k+2})^2 + (i_q^* - i_q^{k+2})^2 \tag{2.23b}$$

$$g_{xy} = (i_x^* - i_x^{k+2})^2 + (i_y^* - i_y^{k+2})^2, \tag{2.23c}$$

However, there are some variations between the techniques. When using virtual-vectors, the x and y errors are not considered because the virtual-vectors are zero in the xy subspace, as shown in [Liu and Liu(2021)]. Another variation is when multi-vector MPC is used. The cost function is applied twice. The first optimal voltage vector is calculated, and another cost function is used to calculate the second. [Yuan

et al.(2020-12)Yuan, Ma, Zhao, and Yang].

The cost function does not change significantly with different techniques. The main difference is the weighting factor for the currents. Some of the papers decided to keep a weighting factor of one for the d and currents and only include a weighting factor for the x and y currents. In general, it is difficult to determine the values of the weighting factors. Many of the articles referenced a paper from 2009 called "Guidelines for weighting factors design in model predictive control of power converters and drives" by Cortes et al [Cortes et al.(2009-02)Cortes, Kouro, La Rocca, Vargas, Rodriguez, Leon, Vazquez, and Franquelo]. The method presented here is to use a branch and bound algorithm to hone in on the optimal weighting factor. Since simulations need to be run to measure the performance metrics, this algorithm aims to reduce the amount of simulations required. Based on other applications of MPC there are some ways in which the cost function for FCS-MPC of a DTP-PMSM can be changed. Villarol et al [Villarroel et al.(2013-02)Villarroel, Espinoza, Rojas, Rodriguez, Rivera, and Sbarbaro] eliminated weighting factors using a multi-objective formulation using multiple cost functions. In a different approach, [Fretes et al.(2022)Fretes, Rodas, Doval-Gandoy, Gomez, Gomez, Novak, Rodriguez, and Dragičević] used a particle swarm optimization algorithm to find the optimal weighting coefficients to reduce xy currents. One of the simplest ways to augment the cost function to add frequency control is to add a variable that tracks the switching states. This is commonly performed in three-phase machines and can be seen in [Sheng et al.(2018-05-31)Sheng, Li, and Ji]. The variable is the sum of the current states, and penalizes a change in

state. This can be seen in,

$$g_i = g_{dq} + \lambda_{xy} \cdot g_{xy} + \lambda_n \cdot n \tag{2.24a}$$

$$g_{dq} = (i_d^* - i_d^{k+2})^2 + (i_q^* - i_q^{k+2})^2 \tag{2.24b}$$

$$g_{xy} = (i_x^* - i_x^{k+2})^2 + (i_y^* - i_y^{k+2})^2 \tag{2.24c}$$

$$n = \sum_{x=1}^{N} |S_x(k) - S_x(k-1)| \tag{2.24d}$$

where S is either 1 or 0; therefore, a change in state is added to the summation. This the inverter frequency. However, when this method is used, the switching frequency remains variable, which is undesirable. Another way the cost function can be used is by adding integrative action. This has been demonstrated in a previous study [Norambuena et al.(2019-12)Norambuena, Lezana, and Rodriguez]. They added a separate weighting factor to the cost function that considers the accumulative error of the states. This adds an integrative action to eliminate the steady-state error. Another simple solution is to add variable references to the cost function. This can be seen in [Yang et al.(2016-03)Yang, Tan, and Hui]; they compensate for the errors in the parameters of a RLC circuit by updating the references at each sampling period. This is a relatively simple way to change the cost function, but it can be effective in reducing the steady-state errors.

2.4.5 Modulation

Modulation is rarely addressed in the literature. For conventional model predictive control a modulator is not used. However, techniques similar to modulation are used in some of new techniques. For example, in variable amplitude virtual-vectors,–which

is a combination of virtual-vectors and a zero vector–after they calculate the optimal times for the vectors, they create a switching pattern with the goal being to keep the switching frequency constant [Gonçalves et al.(2019-02a)Gonçalves, Cruz, and Mendes]. However as discussed by [Wendel et al.(2021-12)Wendel, Karamanakos, Gebhardt, Dietz, and Kennel], by applying multiple vectors in one switching period, the overall current ripples can be reduced. As such, the addition of a modulator can have a large improvement in the steady-state results.

In direct torque and flux control, a common modulation strategy that is implemented is discrete space vector modulation. This can be observed in [Wang et al.(2021-06)Wang, Liu, Liu, and Zhao]. Discrete space vector modulation further splits the output vector into more sections, which allows more vectors to potentially be produced. This increase in precision of the subspace, further reduces the current overshoots in the machine. This technique has also been implemented on three-phase and multilevel inverters as well [Alsofyani et al.(2019-03)Alsofyani, Kim, and Lee] [Lee et al.(2018)Lee, Lee, Moon, and Lee].

2.4.6 MPC Limitations

In the current literature, FCS-MPC MPC suffers from two main problems: steady-state ripple, and steady-state error. The base form of the algorithm only has a proportional effect on the output. It completely relies on the accuracy of the model. If there are errors in the mode, or if it changes in operation the errors will persists. Furthermore, although there have been attempts to choose vectors that minimize the current ripple, the commanded output voltages still produce a lot of current ripple. The novel implementation of FCS-MPC discussed in the next chapter seeks

to eliminate these problems.

Chapter 3

Novel Strategy of Finite Control Set Model Predictive Control for Dual-Three Phase PMSMs

This section will present the novel model predictive control algorithm that was developed for the control of a dual-three phase machine. There are two main contributions that have been made regarding FCS-MPC. The first contribution is using the flux-based model for the calculations instead of the inductance based model. The second is the use of a dynamic control set that varies according to the operating point. The reasoning behind the changes are discussed in the following subsections. Simulation results are also presented that show the advantage of the changes.

The simulations were performed in MATLAB Simulink on a model developed by the Motor Control RTA as part of a joint project between McMaster University and Stellantis. As such, much of the information regarding the model and results will need to be kept confidential. The simulation results are presented in their per unit

values. The per-unit values are based on their max values. For example, if the max current of the machine was 50 A, a per-unit value of 0.5 would be 25 A. In regards to the motor model used for the simulation, the overall inductance's of the motor were less than $1mH$, and its rated speed was 3000 rpm.

3.1 Virtual-Flux Based Model-Predictive Control

The first improvement to the FCS-MPC algorithm is the use of the flux-based model as opposed to the inductance based version. Using the flux-model of the machine simplifies the model and prediction equations used, and allows for a simpler estimation process with a reduced computational load [Preindl(2016), Wendel et al.(2021-12)Wendel, Karamanakos, Gebhardt, Dietz, and Kennel].

To use the flux-based model in the controller, because it is difficult to directly measure the flux, it is required to use a mapping scheme. For simple implementations one can use linear mapping by using a constant inductance. However, for more accurate estimations one can implement lookup tables as well based on finite-element analysis (FEA) or experimental measurement. For this thesis, only constant inductance's were used. However, as demonstrated in the later simulation results, this still results in an improved selection of the optimal vector. A simple diagram comparing the inductance vs flux implementation can be seen in Fig. 3.1.

3.1.1 Flux-based Model

For the predictive model, one can use equation 2.15 that was discussed before. This equation is discretized using the forward-Euler approximation, and the predicted flux

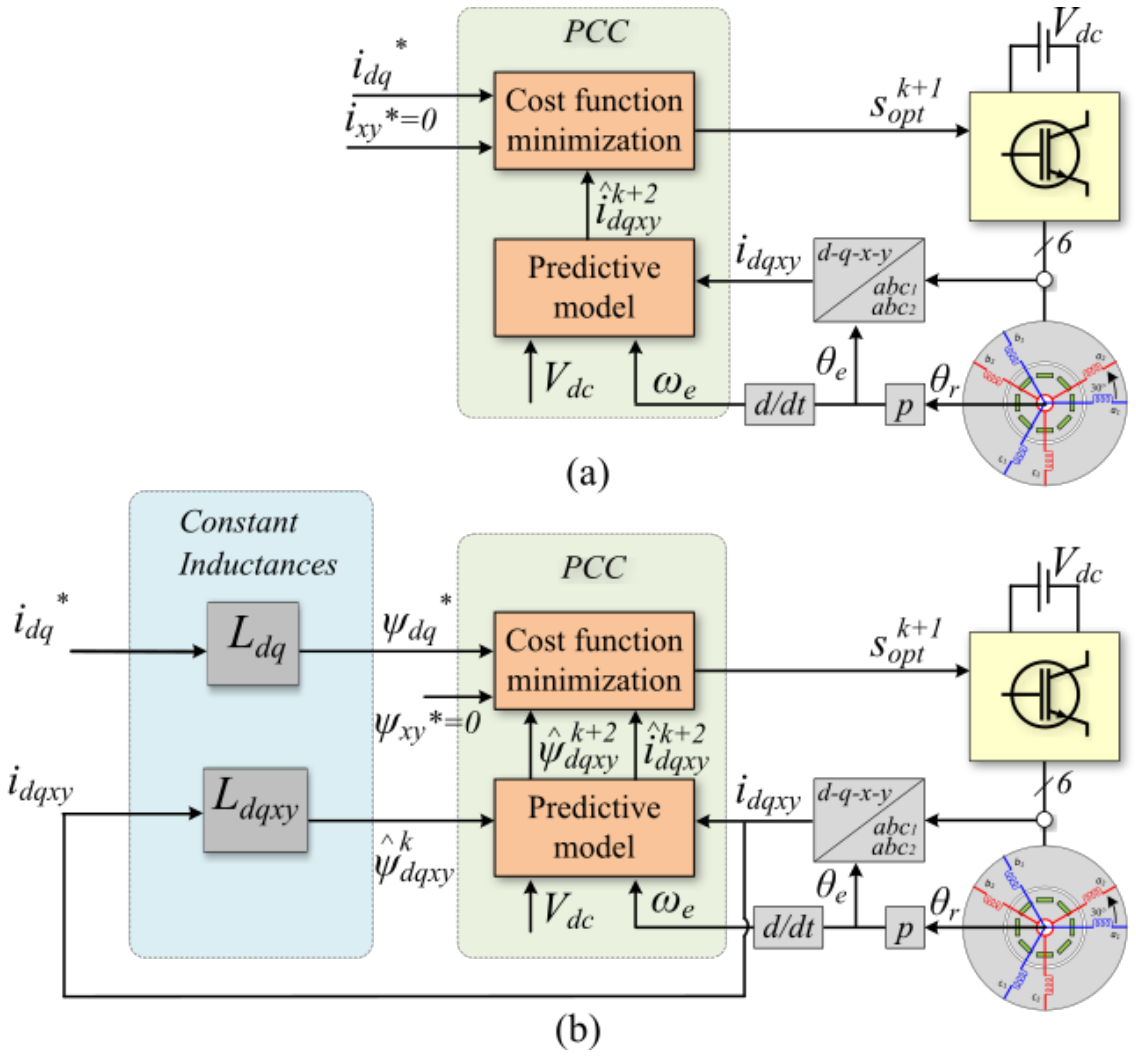

Figure 3.1: Structure of a) Inductance based FCS-MPC Controller and b) Flux-based FCS-MPC controller

can be found. The ψ_{dqxy} equations then become:

$$\psi_d^{k+1} = \psi_d^k + T_s \left[v_d^k - R_s i_d^k + \omega_r \psi_q^k \right] \tag{3.1a}$$

$$\psi_q^{k+1} = \psi_q^k + T_s \left[v_q^k - R_s i_q^k - \omega_r \psi_d^k \right] \tag{3.1b}$$

$$\psi_x^{k+1} = \psi_x^k + T_s \left[v_x^k - R_s i_x^k - \omega_r \psi_y^k \right] \tag{3.1c}$$

$$\psi_y^{k+1} = \psi_y^k + T_s \left[v_y^k - R_s i_y^k + \omega_r \psi_x^k \right], \tag{3.1d}$$

Furthermore, the cost function also becomes based off the flux-linkage, with the reference flux also being found through the mapping.

$$g_\psi = g_{\psi_{dq}} + \lambda_{xy} \cdot g_{\psi_{xy}} \tag{3.2a}$$

$$g_{\psi_{dq}} = (\psi_d^* - \psi_d^{k+2})^2 + (\psi_q^* - \psi_q^{k+2})^2 \tag{3.2b}$$

$$g_{\psi_{xy}} = (\psi_x^* - \psi_x^{k+2})^2 + (\psi_y^* - \psi_y^{k+2})^2, \tag{3.2c}$$

Where λ_{xy}, is a weighting coefficient of the xy currents. If the weighting coefficient is larger, the tracking of the xy currents increases, however, larger errors persist on the other variables.

In this case, for g in (3.2) to achieve the optimum performance, an optimum weighting factor, λ_{xy}^* was found. λ_{xy} is optimized based on the integral-time-square-error (ITSE) performance index of the current loop [Taha et al.(2018)Taha, Beig, and

Boiko]. The optimization problem can be defined as,

$$\min_{\lambda_{xy}} \quad f = \int t\left|\left|e_c(t)\right|\right|_2^2 \, dt \tag{3.3}$$
$$\text{subject to} \quad \lambda_{xy} > 0,$$

where f is the ITSE cost function, $e_c = [e_d \quad e_q \quad e_x \quad e_y]^T$ is the error vector of the dq- and xy-current components, and $||\cdot||_2^2$ is the euclidean norm. The optimization is carried out in Matlab/Simulink using the Nelder-Mead simplex algorithm as a minimax solver [Rao(2009)]. Fig. 3.2 depicts the optimization result using an initial weighting factor $\lambda_{xy} = 1$ and a termination threshold $\epsilon = 0.001$. The optimum weighting factor is then determined as $\lambda_{xy}^* = 1.256$.

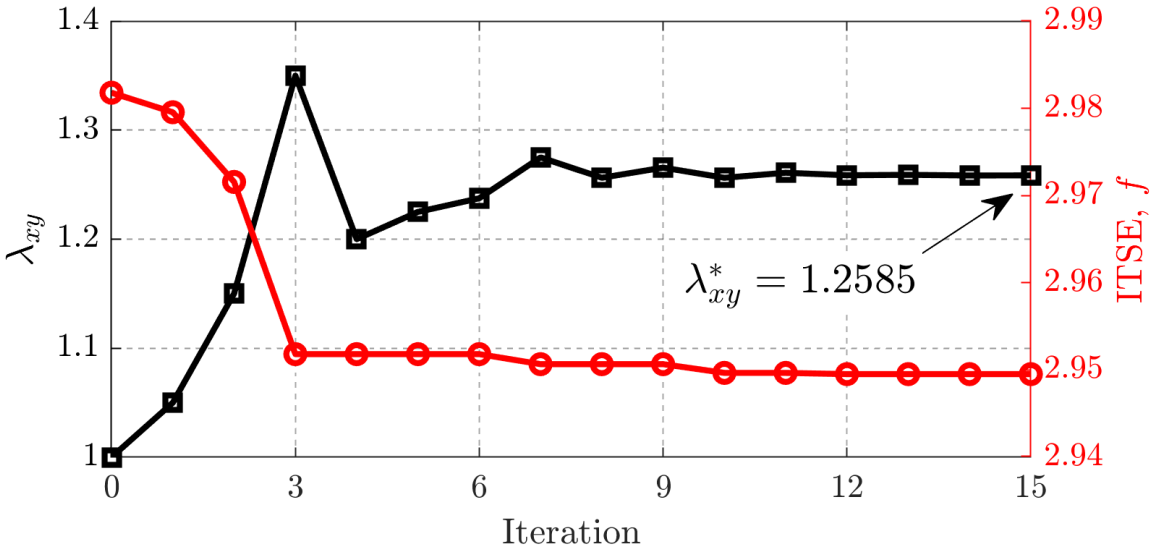

Figure 3.2: Weighting factor optimization showing decision variable λ_{xy} and ITSE cost function f versus iteration count. [Agnihotri et al.(2021)Agnihotri, Valencia, Taha, and Nahid-Mobarakeh]

Table 3.1: Results from Steady-State Simulation at 3000 rpm, $T_{sim} = 0.1s$.

Control strategy	ITSE_{dq}	ITSE_{xy}	ITSE_{T_m}	$\text{THD}_{i_{a1}}$	Mean switching frequency i_{a1} (kHz)
Virtual-flux MPCC	0.203	0.341	0.1858	4.603	2.15
Conventional MPCC	0.231	0.187	0.304	4.29	2.8

3.1.2 Simulation Results - Steady State

To test the performance of the proposed algorithm, several simulations of the algorithm were run. The goal being to investigate if using the flux-based model could improve the control performance compared to the inductance based model. As such, the most basic forms of the algorithms were compared: which considers all 64 vectors in the cost function. For the simulations, the DC link voltage was set at 350 V, and the sampling frequency was set to 20 kHz. The torque reference and speed references were set to their maximum values. The following results were taken from the conference paper published by the author [Agnihotri et al.(2021)Agnihotri, Valencia, Taha, and Nahid-Mobarakeh]. The resulting steady state results can be seen below:

As seen in the table 3.1 and Fig. 3.3, using the flux-based model results in better tracking of the q currents overall, resulting in lower ITSE for the currents and torque. One important thing to note is that MPCC refers to model-predictive current control (MPCC).

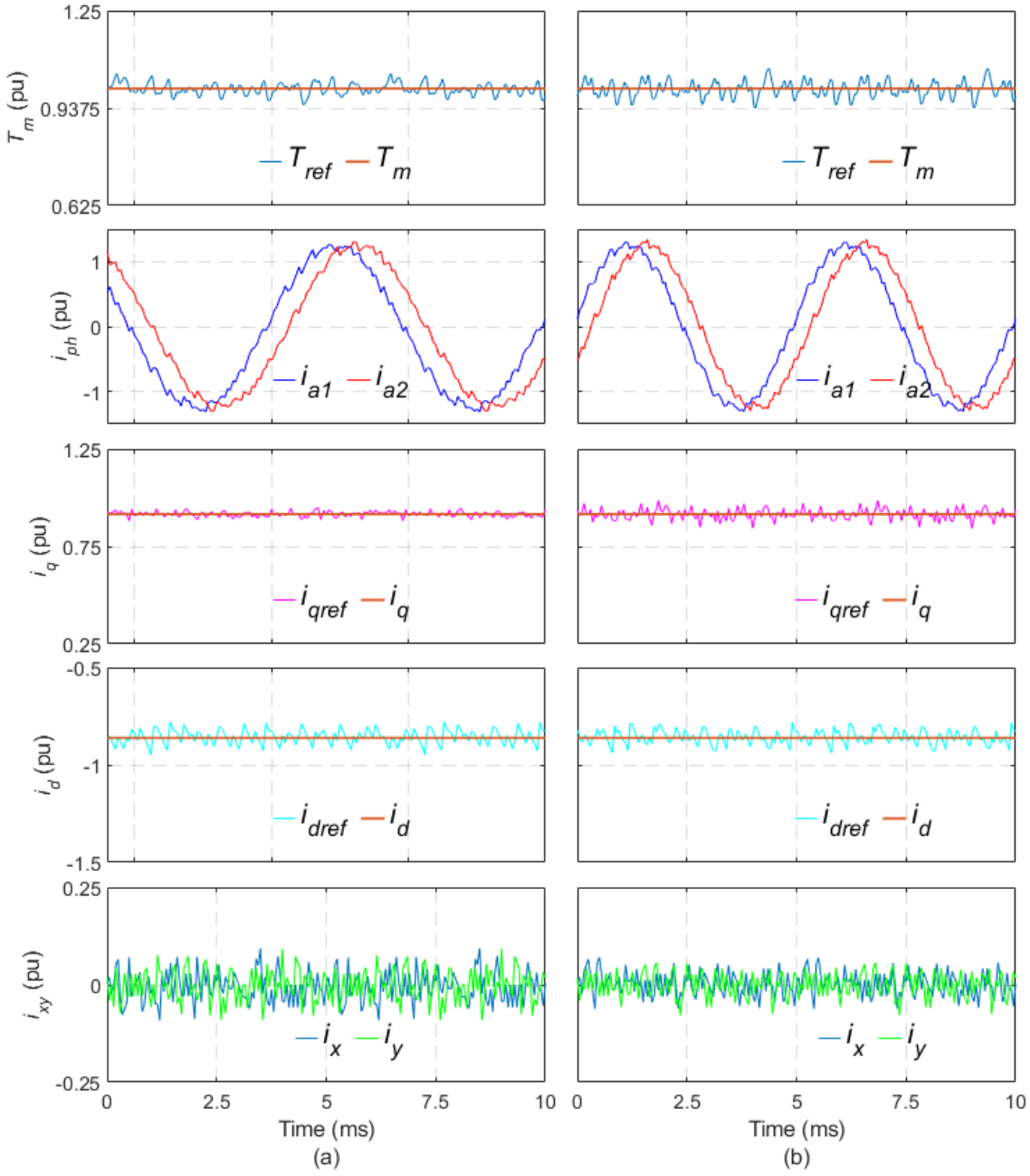

Figure 3.3: Steady-state operation at 3000 rpm (a) Results using virtual-flux PCC (b) Results using conventional PCC [Agnihotri et al.(2021)Agnihotri, Valencia, Taha, and Nahid-Mobarakeh]

3.1.3 Simulation Results - Change in Speed/Torque

Another important test is to see how the algorithms react to changes in the speed and torque. For the speed change test, the speed reference was changed at a rate of 900 rpm/s. For the torque change, the torque reference was changed at a rate of 5000 Nm/s. This coincided with the specifications from the Stellantis team. The resulting plots can be seen in Fig. 3.4 and Fig. 3.5.

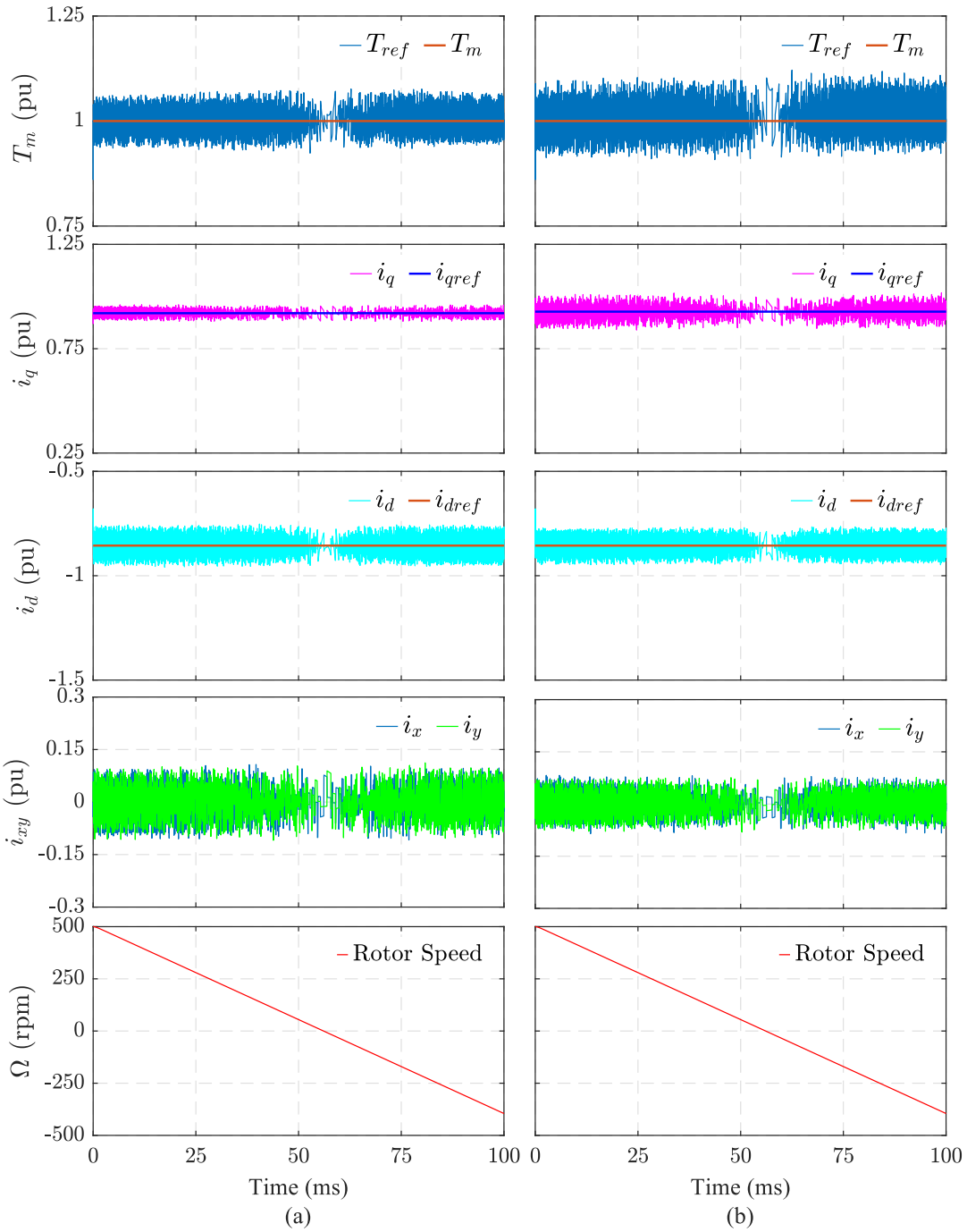

Figure 3.4: Dynamic response for speed change from 500 rpm to -500 rpm (a) Results using virtual-flux PCC (b) Results using conventional PCC [Agnihotri et al.(2021)Agnihotri, Valencia, Taha, and Nahid-Mobarakeh]

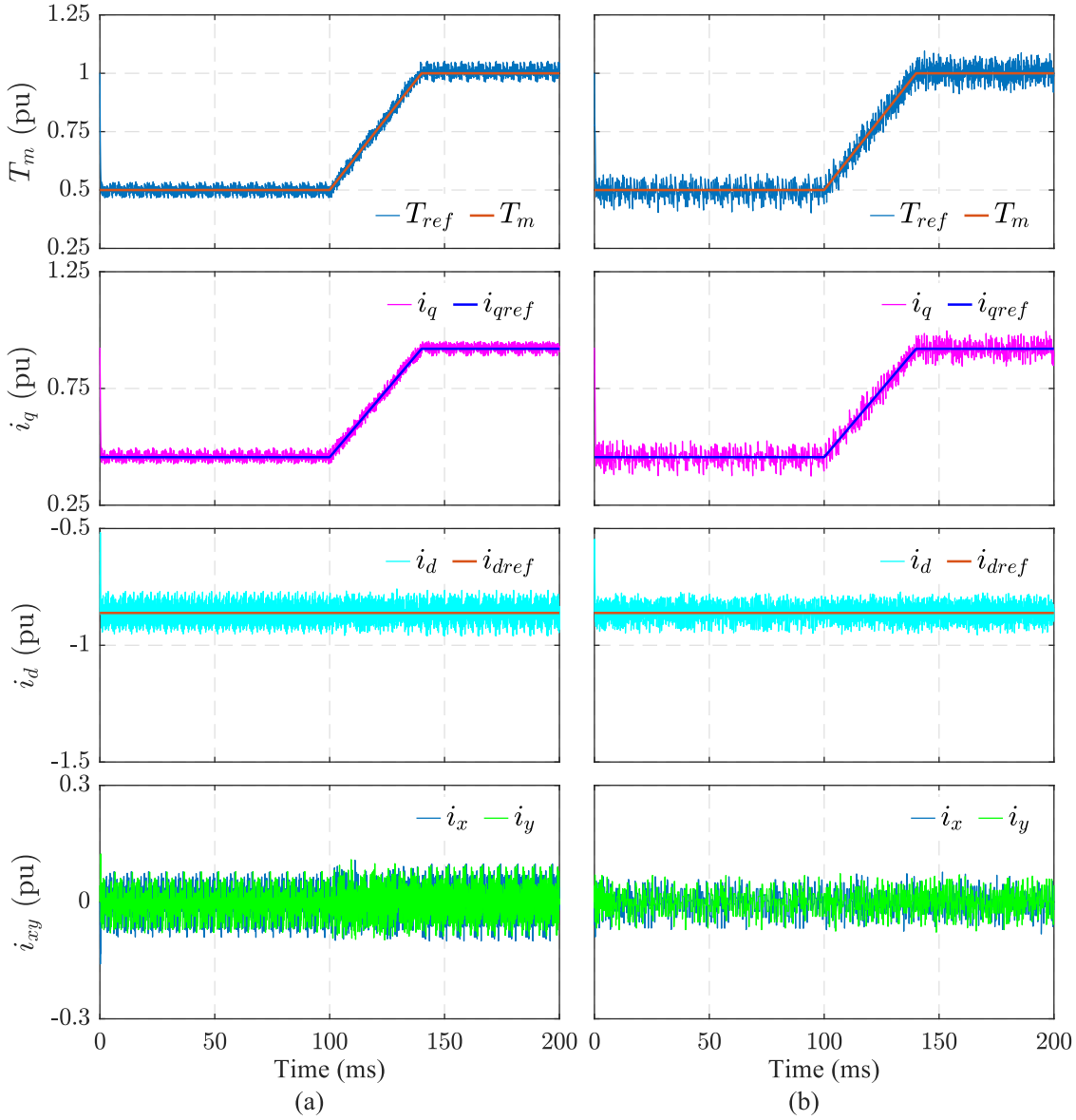

Figure 3.5: Dynamic torque response for a fixed speed of 2000 rpm (a) Results using virtual-flux PCC (b) Results using conventional PCC [Agnihotri et al.(2021)Agnihotri, Valencia, Taha, and Nahid-Mobarakeh]

The results presented in Figures 3.4 and 3.5 show the same results as the steady-state results, in general both models can retain control of the machine even with changes in the speed and torque of the motor. However, the MPC algorithm using

the flux-based model has a better tracking of the q currents, which results in lower torque ripples overall.

One important thing to note however, is that these results were obtained with the machine using the linear equations. This means the non-linearities of the machine such as magnetic saturation and the effects of temperature were ignored. One can still see the advantage of using the flux-based model, however, when using a more accurate model of the motor in the simulations the control performance starts to degrade. Fig. 3.6 shows the results of both algorithms when using the non-linear model of the motor.

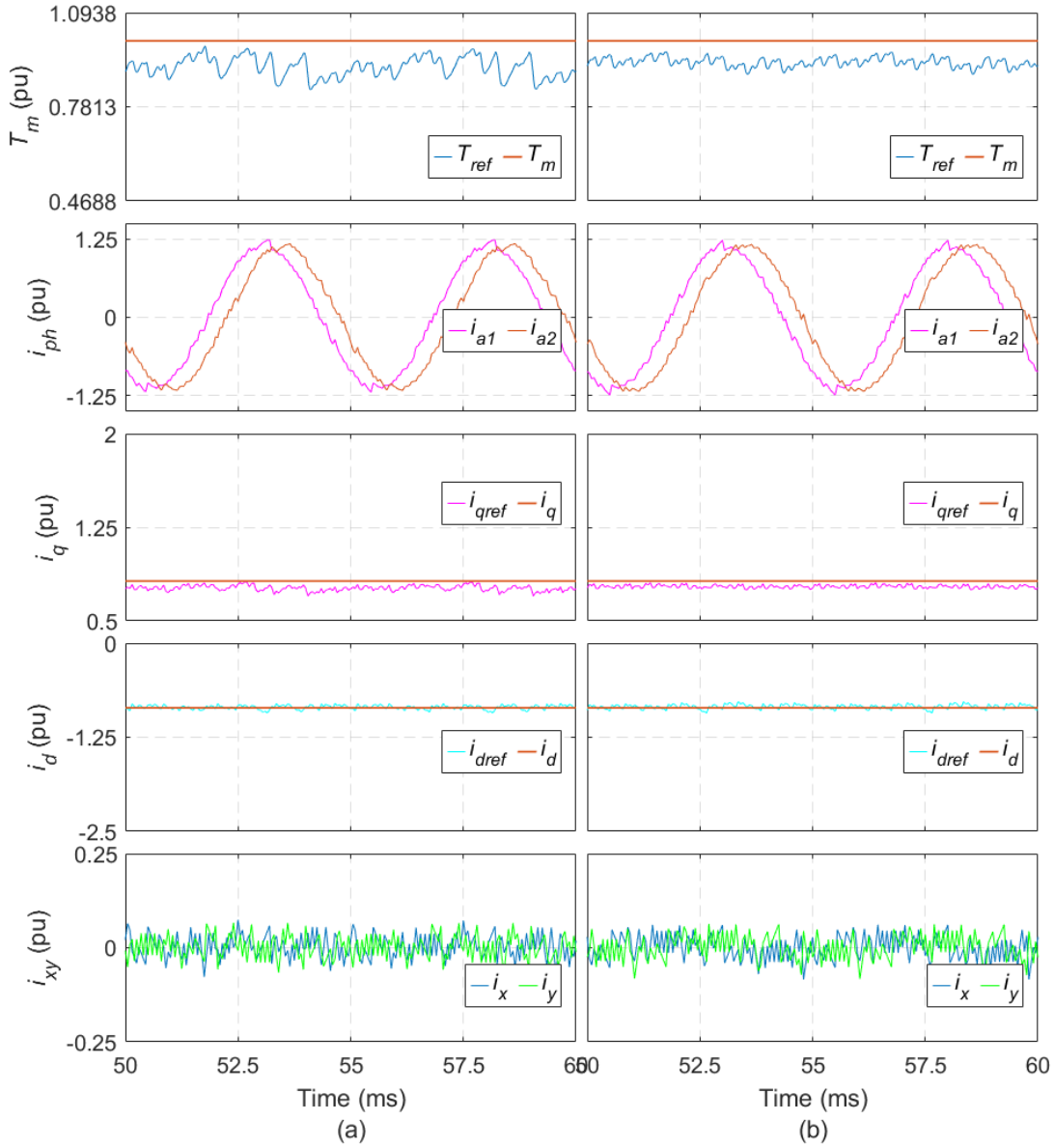

Figure 3.6: Results using the linear FCS-MPC controller with a non-linear Motor Model. Results using a) virtual-flux PCC (b) Results using conventional PCC

As seen in 3.6, when using the basic form of FCS-MPC, if there is mismatch between the model of system and the model used in the algorithm, then there will be

increased errors in the results. This can be corrected by having a more accurate model of the system. Once can accomplish this through creating lookup tables from finite-element analysis or experiments. However, this could require significant memory space depending on how detailed the lookup tables are. Another solution that was discussed in chapter 2 is to create an observer to estimate the parameters of the machine. However, this can be complicated to build, and could require more calculations to be performed.

3.2 Dynamic Finite-Control Set Incremental Model Predictive Control

The modification to the MPC algorithm presented in this section seeks to solve the inherent problems associated with conventional FCS-MPC: the steady state error, and ripple. This is accomplished by introducing the incremental model to the algorithm as well as a dynamic finite control set. A block diagram of the entire algorithm can be seen in Fig. 3.7.

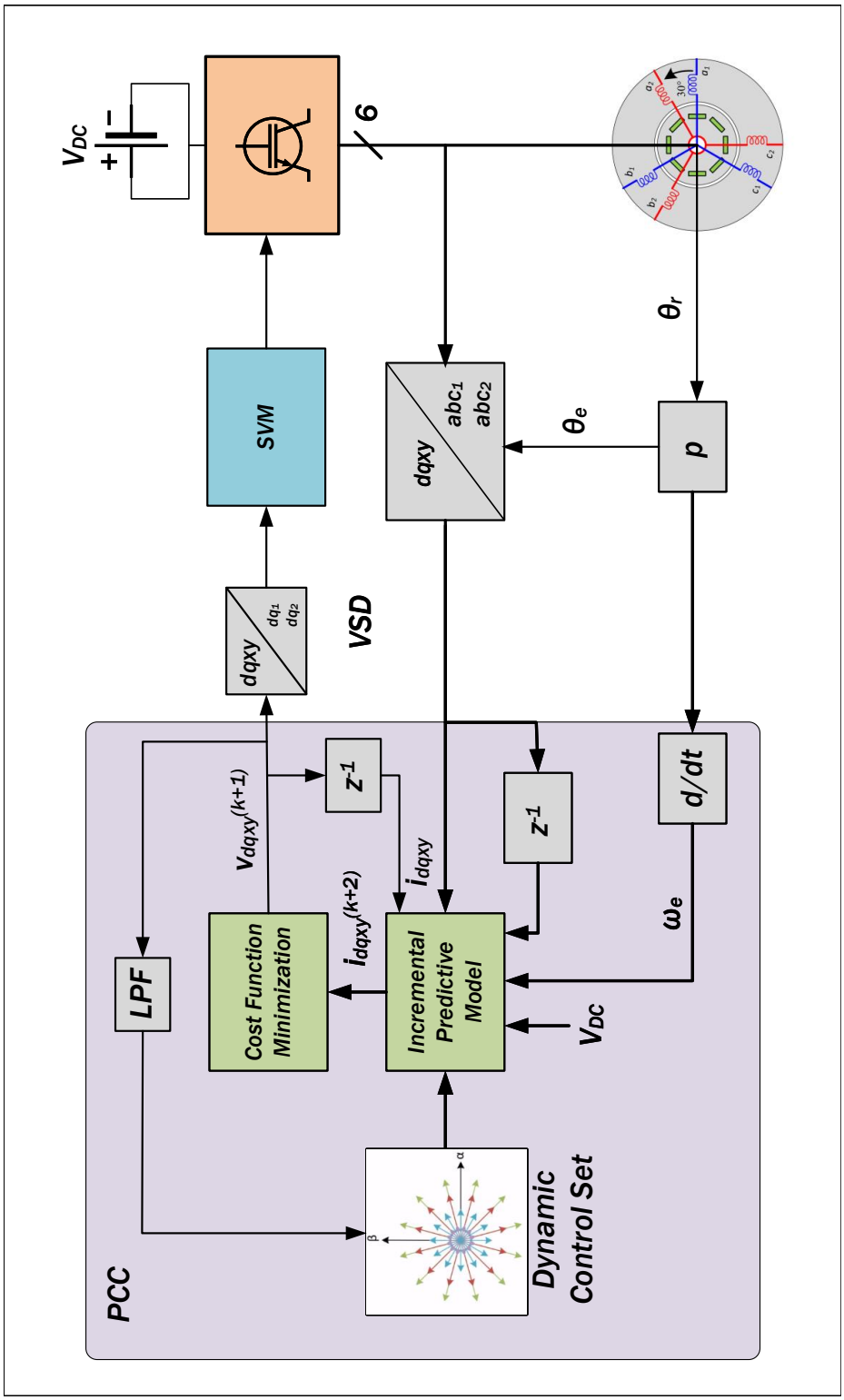

Figure 3.7: Block diagram of Dynamic Control Set FCS-MPC

3.2.1 Incremental Model Predictive Control

The majority of the literature of MPC applied to PMSMs uses the static model of the machine, which considers the measured variables in the present time. However, as described by [Wang(2009)] it is better to use the incremental model of the system includes an integral action into the model, which can eliminate the steady-state errors. In the case of PMSMs it can also eliminate the effects of the permanent magnet flux-linkage. However this is under the assumption that the speed of motor is slowly changing and the sampling frequency is high enough. Consider the state space equations of a three phase PMSM:

$$x(k+1) = Ax(k) + Bu(k) + h \tag{3.4a}$$

$$A = \begin{bmatrix} 1 - R_s\frac{T_s}{L_d} & \omega_e L_q \frac{T_s}{L_d} \\ -\omega_e L_d \frac{T_s}{L_q} & 1 - R_s T_s / L_q \end{bmatrix} \tag{3.4b}$$

$$B = \begin{bmatrix} \frac{T_s}{L_d} & 0 \\ 0 & \frac{T_s}{L_q} \end{bmatrix} \tag{3.4c}$$

$$h = \begin{bmatrix} 0 \\ \frac{\psi_{pm}\omega_e T_s}{L_q} \end{bmatrix} \tag{3.4d}$$

$$x = \begin{bmatrix} i_d(k) \\ i_q(k) \end{bmatrix} \tag{3.4e}$$

$$u = \begin{bmatrix} v_d(k) \\ v_q(k) \end{bmatrix} \tag{3.4f}$$

There exists an extra h term in the model, which just includes the permanent magnet flux-linkage added to the q current.

To use the incremental model instead of the static model, the states x, h, and inputs u are replaced with the differences signified by Δ. As a result of this, if it is assumed that the sampling frequency is high enough such that the states don't change significantly with each successive sampling period, the Δh vector would always be 0. In the end the equation simplifies to:

$$\Delta x(k+1) = A\Delta x(k) + B\Delta u(k) \tag{3.5a}$$

$$\Delta x = \begin{bmatrix} i_d(k) - i_d(k-1) \\ i_q(k) - i_q(k-1) \end{bmatrix} \tag{3.5b}$$

$$\Delta u = \begin{bmatrix} v_d(k) - v_d(k-1) \\ v_q(k) - v_q(k-1) \end{bmatrix} \tag{3.5c}$$

This eliminates one term to the equations, which eliminates one source of error. Furthermore, one can see the block diagram of the new MPC controller in Fig. 3.8. As seen in the diagram the term $\frac{1}{1-q^{-1}}$ is an integrator, which is embedded into the algorithm. This is as opposed to conventional MPC, only has a proportional action to the control.

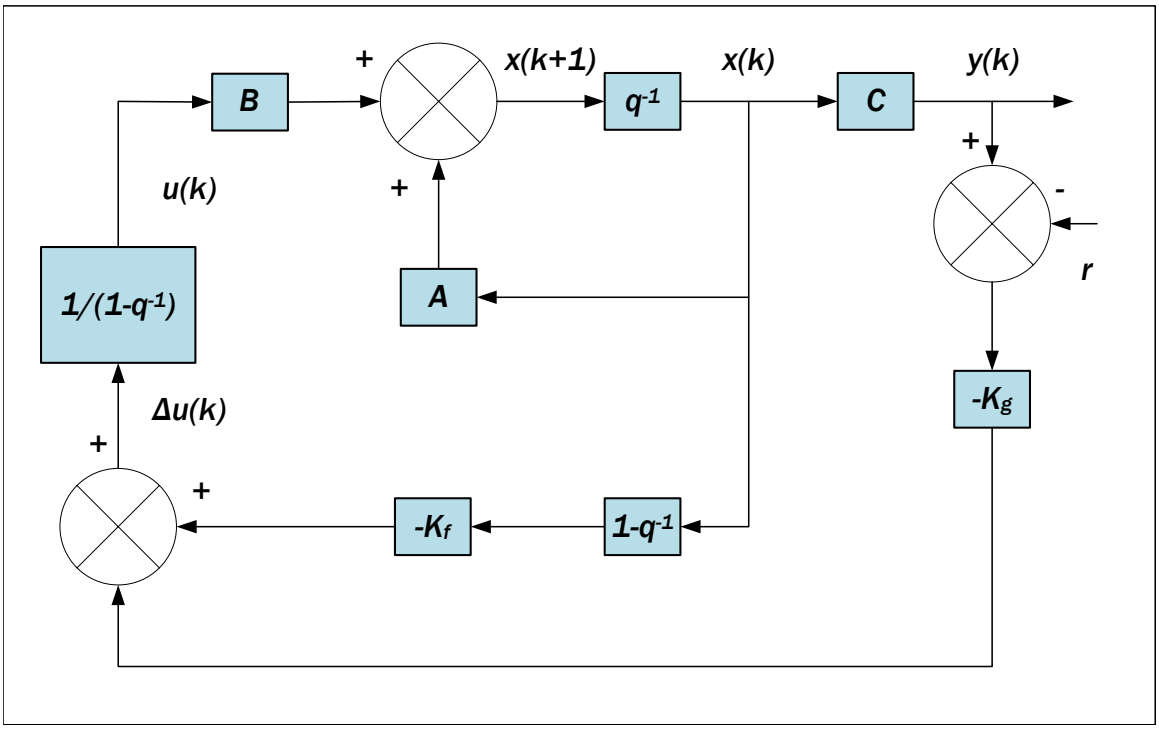

Figure 3.8: State-space model of Incremental Predictive Controller

One important assumption for this algorithm to work is for it to be both controllable and observable. This is assumed to be the case for the rest of the paper.

3.2.2 Dynamic Control Set Strategy

The other improvement that was made was using a dynamic control set. In the literature, when FCS-MPC is implemented they use static vectors: either a subset of the 64 possible vectors, or virtual vectors. However, as discussed before this can still result in significant steady-state ripples in the currents. Especially with a higher DC-link voltage. Furthermore, for a dual-three phase machine it considers the *dqxy* currents under one cost function, therefore, one must balance the control performances of all four currents. This does not take full advantage of the VSD transformation.

The dq and xy sub-spaces are orthogonal to each other, therefore, one should be able to consider them separately in the cost function.

The dynamic control set seeks to alleviate these issues. The strategy is to continually update the candidate vectors. Although this requires the use of a modulator, it allows for a more accurate vector to be chosen with significantly better current ripples. The principle of the technique is illustrated by Fig. 3.9. If the current references do not change much, then the v_{dq} references should not change much at all. Therefore, the search space can be narrowed to a small area. The principle is to start with a very broad vector search space, and then narrow it down with time. As time passes, the search space will reach a very precise value, which has significantly less overshoot.

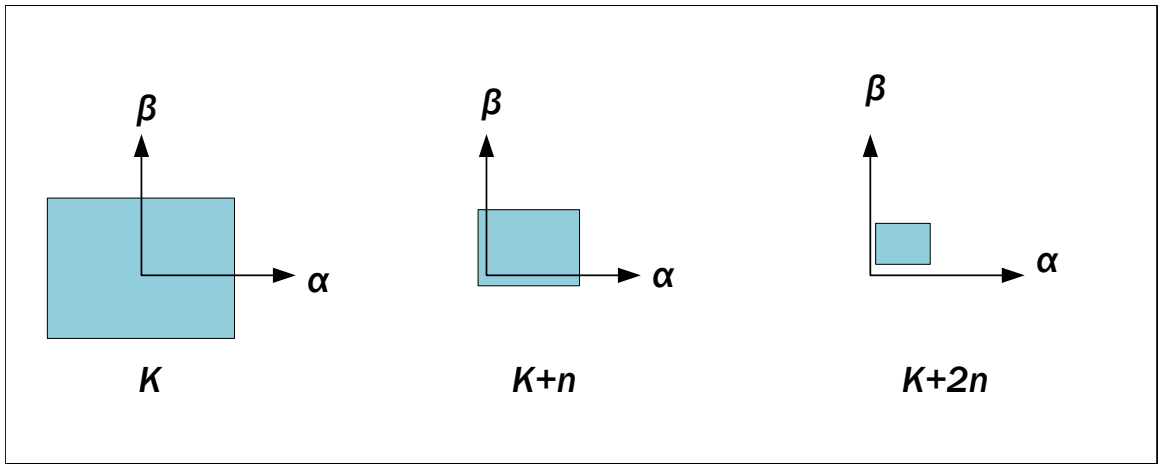

Figure 3.9: Example of Dynamic Subspace. It is updated every n time steps

The implementation of this concept is straightforward. The following explanation will be about the dq currents, however, the same process can be applied to the xy currents as well.

The first step of the process is to create the search space. At the start of the

controller being turned on, one should use a broad search space that covers the range of the modulator. This search space is created based off a pivot vector, which is essentially the center of the search space. Eventually the pivot vector becomes very close to the "true" optimal value. At first, this pivot vector is set to 0. The range of the search space was set to $0.3Vdc$. In general, if the voltage search space is too small the value will not be able to converge to the proper value, if the value is too large then there will be large overshoots. The value of $0.3Vdc$, is arbitrary but it was found to give a quick response with low overshoot.

After the range was chosen, the search space was created. This was done by evenly spacing the α and β voltages. The amount that one wants to space them is up to preference. Having more vectors to choose from will give a value closer to the optimal one, however, more computations will need to be performed. For this application a search space of 25 vectors was created for each iteration. This is much less than the 64 vectors used for basic FCS-MPC, so should require less computational time.

After the search space is created, it is fed into the incremental predictive model and cost function, which finds the dq voltage to implement by iterating through each vector. This is then fed into the modulator, which implements the voltage vector.

At the same time the output vector is filtered and fed back into the dynamic-subspace equation. The output of the filter becomes the new pivot vector. This allows the pivot vector to become closer and closer to the true optimum value. A filter was needed because of the discretization of the search space. Since there is very small group of vectors the resulting overshoot is fairly large. Adding the filter removes the overshoots from this. The transfer function of the filter used was:

$$H(s) = \frac{1}{1/1000s + 1} \tag{3.6}$$

The cutoff frequency used for this machine was 1000 rad/s. It was found through trial and error. It is much higher than the rated frequency of the machine, so allows for a quick convergence to the optimal vector.

The range of the vector search space was updated every 10 samples. It was found that if was updated too fast, the response time of the controller was affected, while if it was too long, there would be larger overshoots and longer settling time. After 10 samples, if the difference between the reference and optimal vector is greater than 2.5 the range is cut in half, with the floor value being 2.5 V. This is a simple but effective way for reducing the range.

3.2.3 Simulation Results

Similar to the flux-based MPC before, this algorithm was first tested in simulation. Both the flux-based and inductance-based dynamic subspace MPC algorithms were created.

However, for these simulations to prove the steady-state error compensation capability of the new algorithms, the non-linear model of the machine was used in the simulations. The non-linear model of the machine uses non-linear flux linkages from lookup tables based on finite element analysis.

The results are shown compared to the basic flux-based MPC algorithm. The first test that was done was a steady state test. The motor was run at its rated speed and torque. This result can be seen in Fig. 3.10, as well as table 3.2. Using the incremental model with the dynamic vector space allows the steady-state results to

Table 3.2: Results from Steady-State Simulation at 2000 rpm, $T_{sim} = 0.1s$.

Control strategy	ITSE_{dq}	ITSE_{xy}	ITSE_{T_m}	$\text{THD}_{i_{a1}}$
Virtual-flux MPCC	21.0	15.3	64.4	4.603
Dynamic Incremental Inductance MPCC	1.58	0.000791	1.72	1.54
Dynamic Incremental Flux MPCC	1.62	0.000790	1.58	1.53

be significantly improved compared to conventional MPC. The steady state errors are eliminated in all of the currents, which improves the ITSE of all the currents and torque. When comparing the inductance based version and the flux based version, the results were extremely similar. Although the flux-based version had a slighlty better ITSE with the torque. This is because it had slightly better tracking of the d currents, which resulted in lower torque ripples.

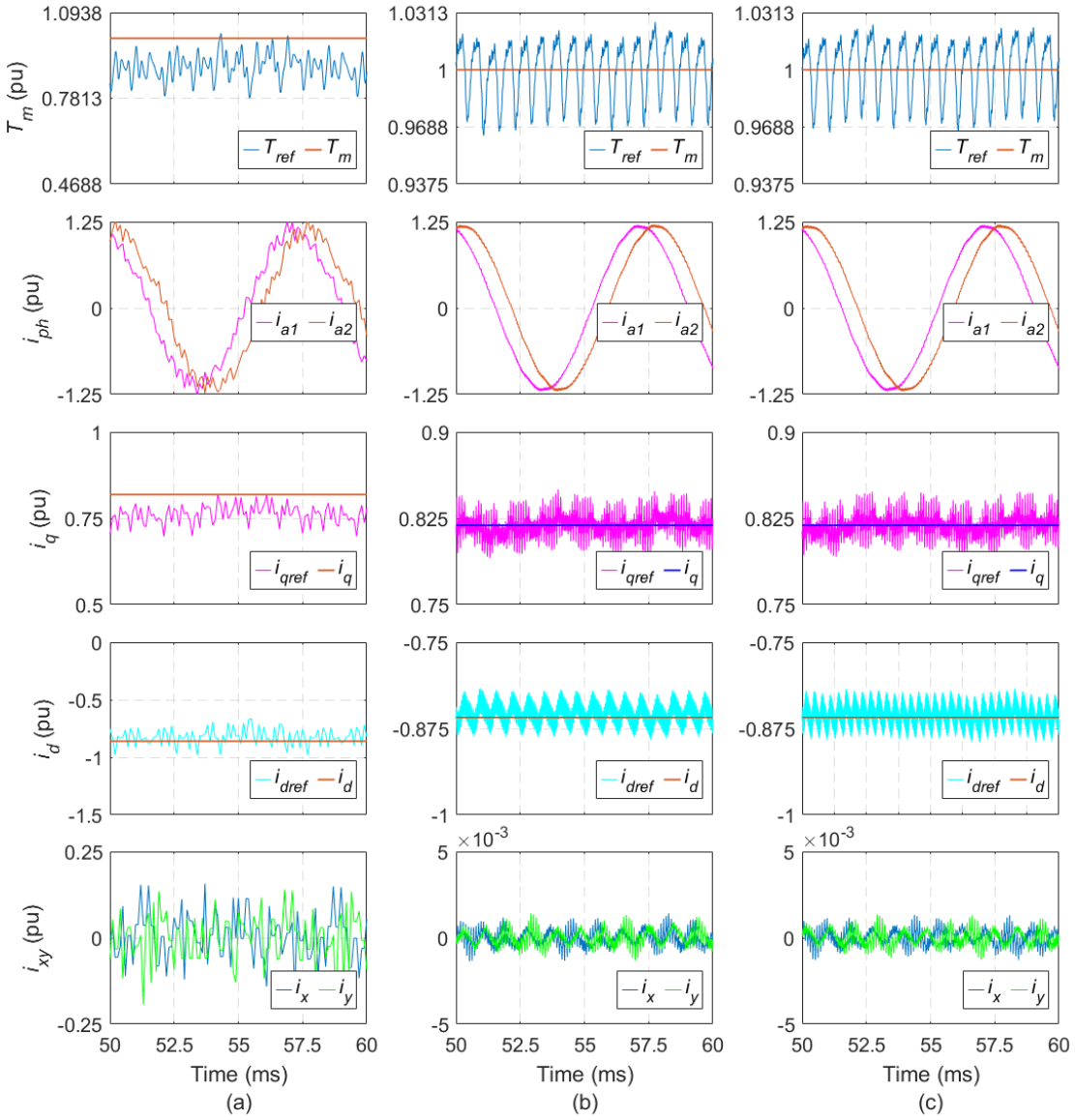

Figure 3.10: Results using the linear model for FCS-MPC with a non-linear Motor Model. Results using a) virtual-flux PCC (b) Results using Dynamic Subspace FCS-MPC c) Using dynamic subspace virtual-flux PCC

The other advantage of the proposed algorithm is improved performance even

with low currents. When using model predictive control, the xy currents tend to stay the same RMS value no matter the dq reference. Therefore, at very low currents, the THD of the phase currents is significantly worsened. However, since the proposed method uses a modulator, it can get more accurate references, even at low current reference. This can be seen in Fig. 3.11 and table 3.3. Even at a low reference currents the ITSE is low, resulting in reduced torque ripples and steady-state error.

Table 3.3: Results from Steady-State Simulation at 2000 rpm, $T_{sim} = 0.1s$.

Control strategy	ITSE_{dq}	ITSE_{xy}	ITSE_{T_m}	$\text{THD}_{i_{a1}}$
Virtual-flux MPCC	8.09	19.06	10.1	44.2
Dynamic Incremental Inductance MPCC	0.306	0.000610	0.2172	3.74
Dynamic Incremental Flux MPCC	0.288	0.000611	0.199	3.67

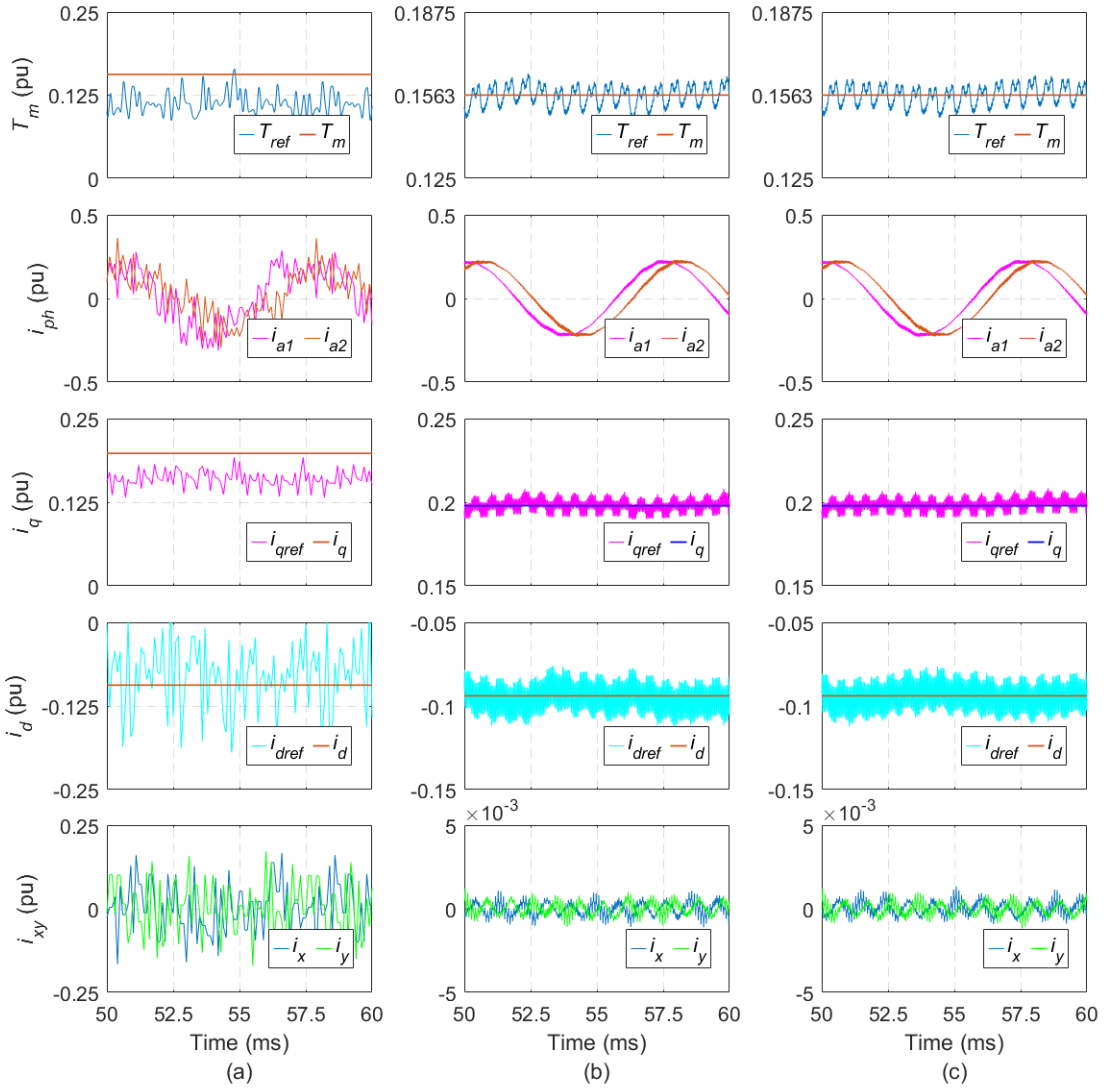

Figure 3.11: Results using the linear model for FCS-MPC with a non-linear Motor Model. Results using a) virtual-flux PCC (b) Results using Dynamic Subspace FCS-MPC c) Using dynamic subspace virtual-flux PCC

The other important aspect of the algorithm is the tolerance to modelling errors. The incremental model eliminates the need for the permanent magnet flux-linkage

and it also has tolerance to some modelling errors. To test this, 20% errors were added to the inductance's, resistances, and permanent magnet flux-linkage. As seen in Fig. 3.12 and table 3.4, the performance of the proposed algorithms stay relatively the same, while the performance of the conventional MPC-algorithm degrades considerably.

An important thing to note in the results of all of these simulations is that the dynamic subspace flux-based model has a slightly better performance than the inductance based version, but the differences are very small. However, no matter which model is used, the benefits of adding the incremental model as well as the dynamic subspace can be seen. The proposed method has been validated through simulation, the next chapter shows the validation on an experimental setup.

Table 3.4: Results from Steady-State Simulation at 2000 rpm, $T_{sim} = 0.1s$.

Control strategy	ITSE_{dq}	ITSE_{xy}	ITSE_{T_m}	$\text{THD}_{i_{a1}}$
Virtual-flux PCC	897	30.8	3600	8.91
Dynamic Incremental Inductance PCC	1.71	0.000791	1.72	1.56
Dynamic Incremental Flux PCC	1.60	0.000781	1.77	1.54

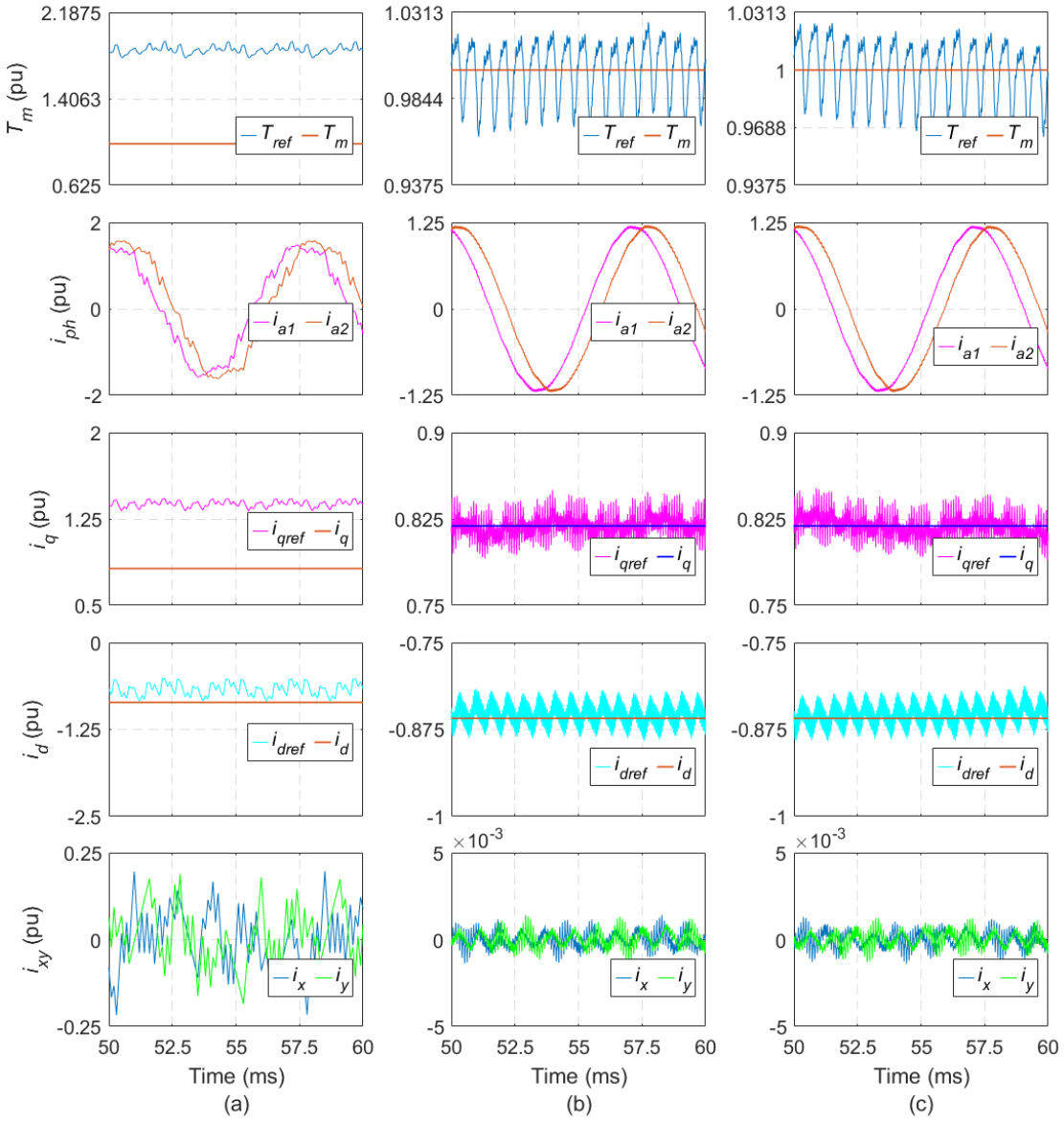

Figure 3.12: Results using the linear model for FCS-MPC with 20% error on the inductances. Results using a) virtual-flux PCC (b) Results using Dynamic Subspace Inductance FCS-MPC and c) Using dynamic subspace virtual-flux PCC

Chapter 4

Experimental Implementation

This section details the results from implementing the algorithm on an experimental setup. First the setup will be introduced, as well as the embedded system that was used to create it. Then tests to measure the performance of the algorithms will be presented.

4.1 Experimental Setup

A picture of the experimental setup can be seen in Fig. 4.1. The setup consists of a dual-three phase PMSM with the shaft connected to a torque sensor and three-phase motor. The three-phase motor controls the speed of shaft while the DTP-PMSM applies the load.

The three phase motor was controlled by a PM150 inverter, which is a commerical inverter purchased from Cascadia motion. The MicroLabBox acts as the central controller of the setup. It commands the speed of the PM150 over CAN and also fully controls the 6-ph setup. It reads the values from all the sensors, performs all

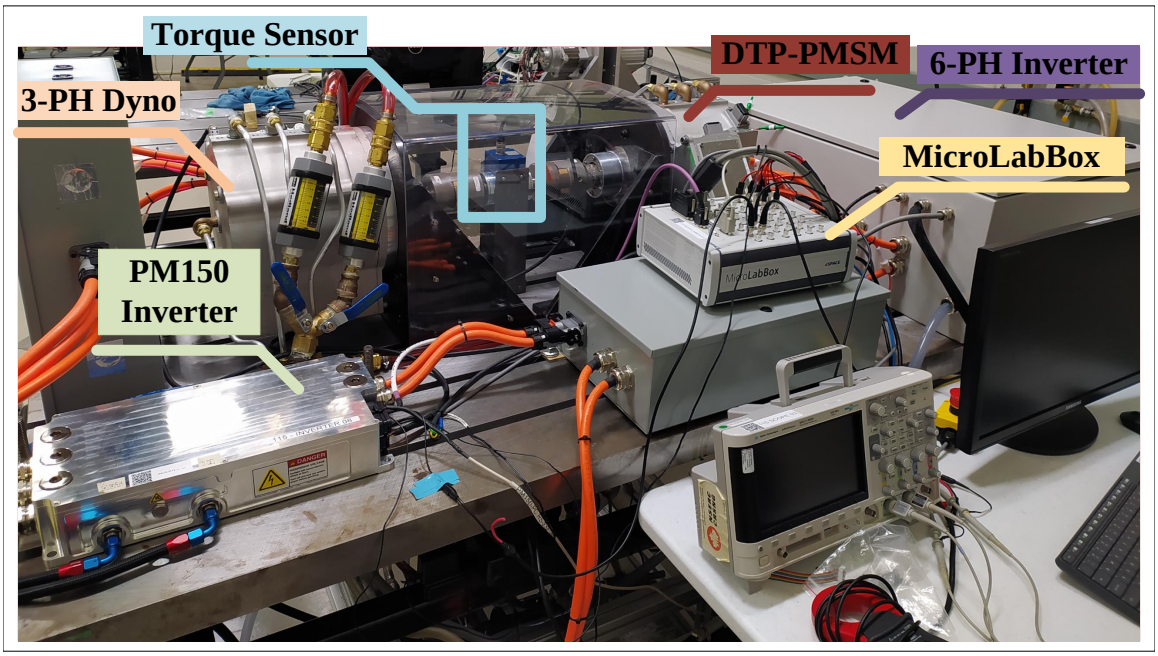

Figure 4.1: Picture of Experimental Setup

of the necessary calcualtions, and sends the pulses to the gate drivers of the 6 phase inverter. The six-phase inverter includes 6 dual IGBT modules connected to commercial gate drivers. The gate drivers accept TTL PWM signals from MicroLabBox, which determines when the legs of the inverters are switches on.

4.2 dSPACE MicroLabBox Platform

The program was implemented in on the MicroLabBox platform from dSPACE. The dSPACE platform is a system that allows easier implementation for hardware in the loop (HIL) setups. The dSPACE platform includes multiple processors and FPGA modules with a 2 GHz clock signal to allow for implementation of fast control algorithms. It also includes custom Simulink blocks as well as C-compilers that convert

Simulink programs to C code. As such, one can easily implement the programs developed in Simulink to the HIL setup.

To communicate between the host PC and the MicroLabBox a graphical user interface was developed. This was created in Control Desk, which is part of the dSPACE package. The various types of the MPC algorithms as well as the PI controller was developed for the dSPACE platform and then implemented.

Similar to the simulations performed, multiple steady-state and dynamic tests were performed to test and compare the algorithms.

4.3 Experimental Results

4.3.1 Modified Dynamic Subspace MPC

In testing the steady state results for the dynamic subspace MPC it was found that the controller was able to control all of the currents effectively except the x currents. The x current control also became worse with higher speeds. To illustrate this, Fig. 4.2 shows the steady state results with the speed of the motor set to 3000 rpm. This implies that the motor model for the x current is not complete. In light of this, it was decided that for the dynamic subspace MPC, it would only be used for the dq currents, while a PI controller would be used for the xy because the PI controller produced lower currents in the xy subspace, which is better for the harmonic content of the currents. In general, MPC has a better dynamic response when compared to conventional PI controller. Because the xy references will always remain at zero, this was seen as a reasonable compromise.

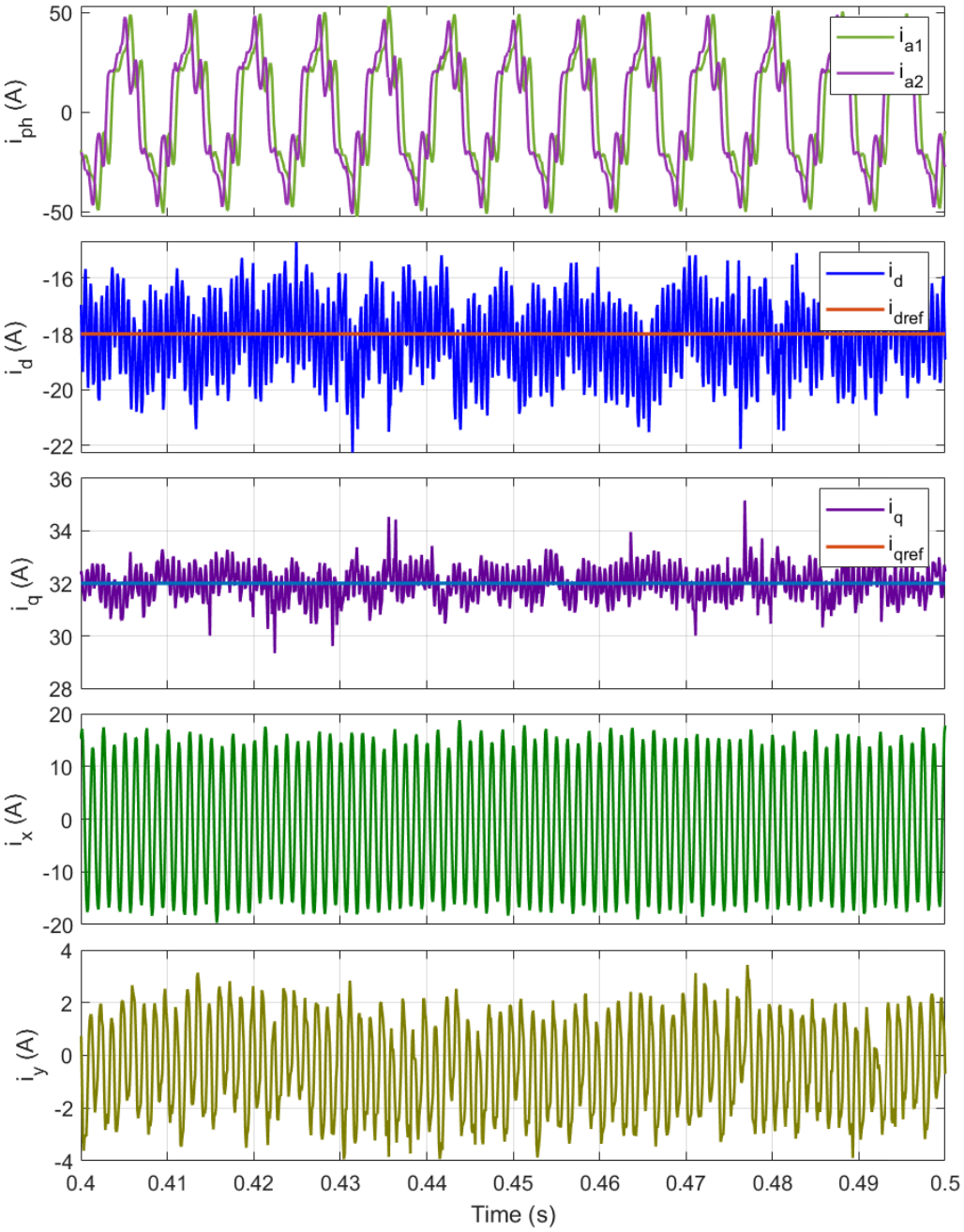

Figure 4.2: Steady-state Results of Inductance Based Dynamic MPC at 2000 rpm illustrating the difference in the xy currents

4.3.2 Steady-state Results

The first tests that were done was the steady state results. The same current references were used for each algorithm. Four speeds were used in this test: 500 rpm, 1000 rpm, 1500 rpm, and 2000 rpm. This should give a good idea of how each algorithm performs at a wide range of operating points. The parameters of the algorithms were the same as the simulations. For the PI controller, the gains can be summarized in table 4.1. The gains were calculated using the pole-zero compensation method described in chapter 2.2.3. It also included decoupling as described in Fig. 2.4.

Table 4.1: Parameters used in PI controller based on pole-zero compensation

PI Parameter	Value
Kpd	0.4841
Kid	112.5
Kpq	1.692
Kiq	112.5
Kpx	2.25
Kix	202.5
Kpy	2.25
Kiy	202.5

An example of the steady state results at 1000 rpm can be seen in Fig, and the results at different speeds is summarized in table 4.2. The first thing to note is that using PI controllers produces the best steady state results at all speeds. This is

expected as in general PI controllers have very good tracking in the steady-state.

Table 4.2: Comparison of Steady State Results

Control Strategy	**Speed**	**ISEd**	**ISEq**	**ISEx**	**ISEy**	**THDa1**
PI	500	0.1840	0.1372	0.2856	0.2778	2.08
	1000	0.1224	0.1464	1.5490	1.5075	3.74
	1500	0.1524	0.1373	4.1643	4.0965	5.87
	2000	0.2122	0.1439	9.9277	9.8464	8.95
Dynamic Subspace Inductance MPC	500	0.2594	0.2031	0.2907	0.2859	2.29
	1000	0.2782	0.2201	1.3278	1.2982	3.58
	1500	0.2761	0.254	3.4394	3.4066	5.46
	2000	0.2545	0.2213	8.7968	8.7999	8.39
Dynamic Subspace Flux MPC	500	0.2483	0.1982	0.2962	0.2875	2.41
	1000	0.2674	0.2341	1.5477	1.5029	3.86
	1500	0.246	0.2442	4.0933	4.0459	5.86
	2000	0.1967	0.2196	9.7449	9.662	8.98
Conventional Flux MPC	500	57.3568	16.8951	484.5049	561.4412	66.40
	1000	56.1812	13.1778	408.5284	449.2175	61.10
	1500	84.2133	13.0737	411.36	453.1741	69.24
	2000	117.8563	14.1829	399.5834	439.6129	58.89
Conventional Inductance MPC	500	55.7722	66.8943	709.4914	597.4914	53.43
	1000	74.8414	131.3655	1994	2038	71.19
	1500	–	–	–	–	–
	2000	–	–	–	–	–

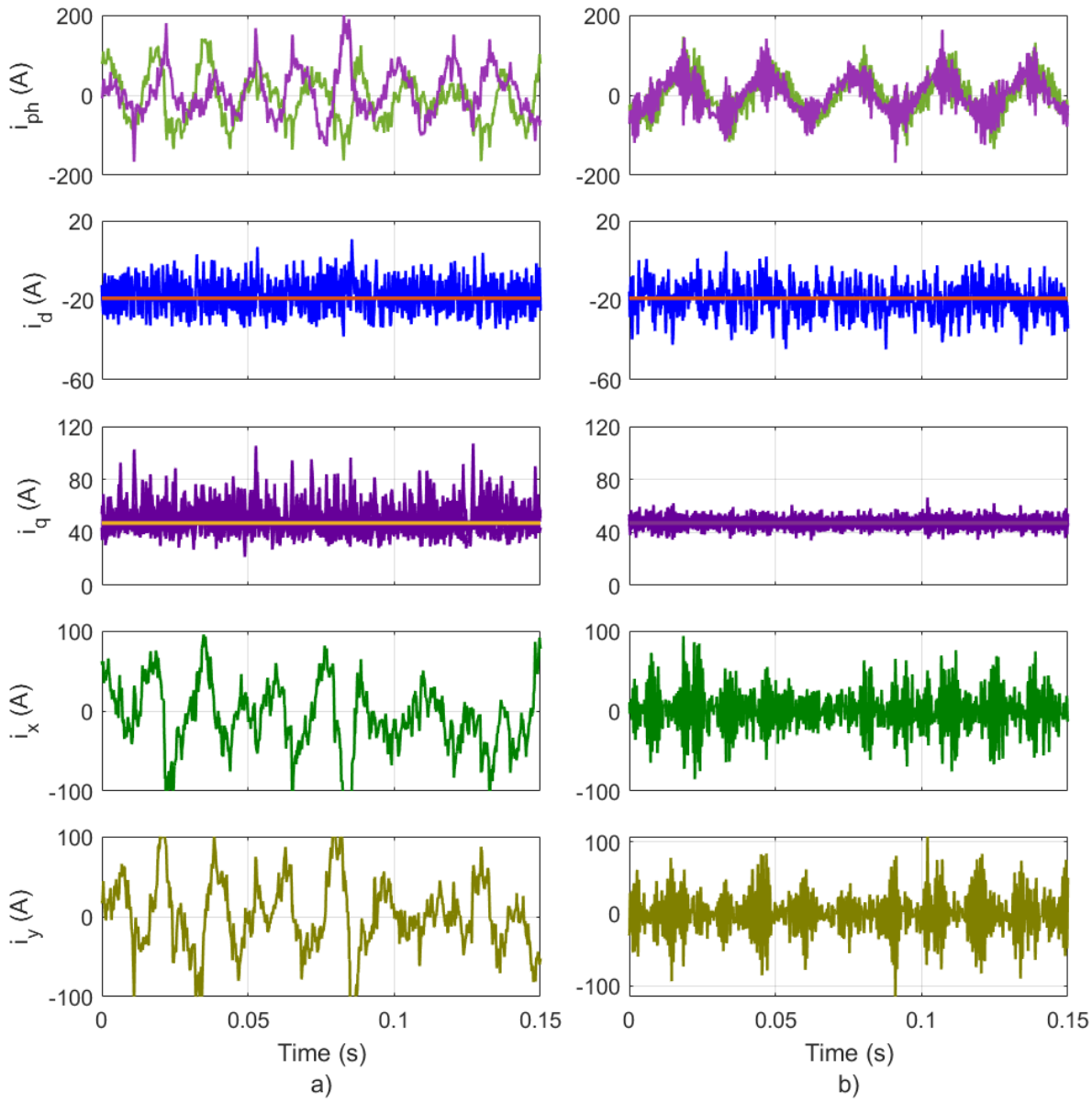

Figure 4.3: Steady State Results comparing: a) Conventional Inductance Based MPC and b) Flux-Based MPC at 1000 rpm

The current tracking of the conventional methods can be seen in Fig. 4.3. In regards to the MPC algorithms, the conventional flux-based MPC algorithm has

a much lower steady-state ripple compared to the conventional inductance based version. The current ripple for the inductance based version was so large that it caused the current limit to be reached on the DC power supply that was being used to run the experiments. As such, the results are missing at higher speeds. However, this still shows that using the flux-based model can produce significantly better performance for the MPC controller when using the conventional subspace.

The results comparing the PI controller steady results and the proposed MPC algorithms can be seen in Fig. 4.4.

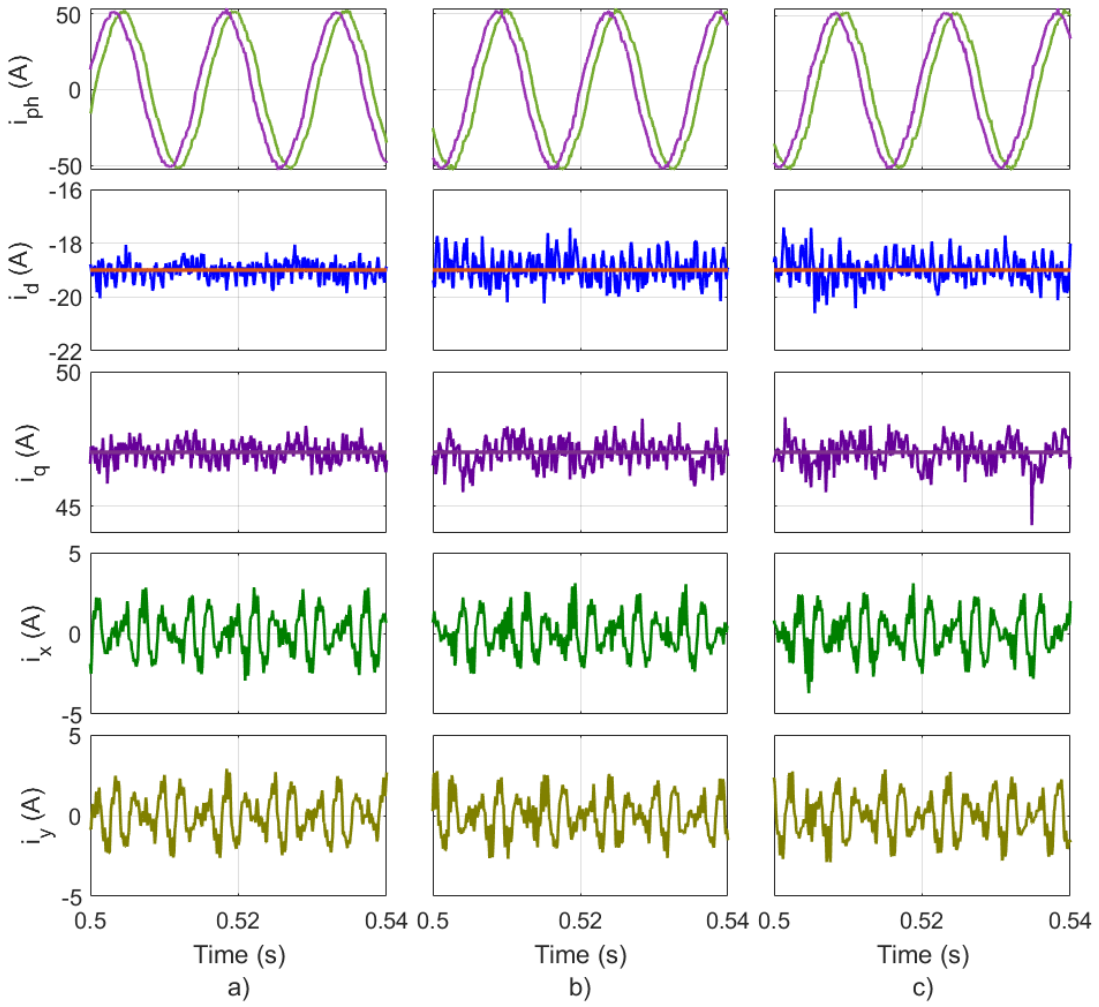

Figure 4.4: Steady State Results comparing: a) PI b) Dynamic Inductance MPC c) Dynamic Flux MPC at 1000 rpm

One important note is that compared to the conventional MPC algorithms, using the dynamic subspace MPC produces significantly better steady state results in terms of integral squared error (IAE). Both the inductance based version as well as the flux-based algorithms have a steady state result comparable to PI controllers. This results in an overall low THD.

Table 4.3: Execution Times of Each Control Strategy

Control Strategy	Execution Time (μs)
PI	15.57
Dynamic Subspace Inductance	19.31
Dynamic Subspace Flux MPC	19.30
Conventional Inductance MPC	22.69
Conventional Flux MPC	22.30

Another important comparison is the execution times of the algorithms. This is especially important for model-predictive control of multi-phase machines because the increased number of phases causes exponentially more calculations to be performed. As seen in table 4.3, the proposed methods have less computational time than the conventional methods largely attributed to the reduced number of vectors in the dynamic subspace. PI controllers had the fastest execution time, which is to be expected since the equations to implement it are relatively simple.

Furthermore, it can be seen that the dynamic inductance MPC seemed to have better control over the xy currents at higher speeds. It is unknown why this is the case because xy currents were controlled by a PI controller, so they should have the

same results. This result should be investigated further, but at this point it is beyond the scope of this paper.

Although the IAE of the dynamic MPC results are higher than the PI controllers this is still seen as a good improvement towards the conventional algorithm. Furthermore, generally has a better dynamic response when compared to PI controllers and this will be further discussed in the next section.

4.3.3 Step Response

The purpose of this algorithm is to develop a good controller under all operating conditions. In a vehicle, depending on the situation the torque–and as such the current reference–will be changing a lot. Therefore, the response time to changes in references is very important. To test how the algorithm responds to such changes, the step response of the PI and dynamic MPC algorithms was compared. A step change in both the Id and Iq currents was applied and the currents were measured. The step change results can be seen in Fig. 4.5 and table 4.4. As seen in the figures, if the references for id and iq are changed at the same time, the id current experiences some lag in the response. This allows the flux based dynamic MPC to have a better integral time squared error (ITSE) compared to the PI controller. Furthermore, as seen in the rise and fall times of the algorithms, the dynamic MPC algorithms have a faster response time to the reference change. This implies that at higher changes in reference, the dynamic MPC will be able to track the changes better when compared to the PI controller. However, still there needs to be more work in improving the error as the PI controller was able to have less overshoot when compared to the dynamic MPC controllers.

Table 4.4: Comparison of Step Response Results

Control Strategy	**Speed (rpm)**	**ITSEd**	**ITSEq**	**ITSEx**	**ITSEy**	**Fall Time id (ms)**	**Rise Time iq (ms)**
PI	1000	1.372	0.282	4.649	4.613	1.23	1.03
	1500	3.301	0.501	12.509	12.690	1.8251	1.3466
Dynamic Ind MPC	1000	1.223	0.401	4.884	4.921	0.2489	0.6419
	1500	1.762	0.462	10.214	10.045	0.2270	0.6510
Dynamic Flux MPC	1000	1.210	0.401	4.420	4.139	0.2423	0.5218
	1500	1.765	0.435	10.309	10.132	0.1374	0.6431

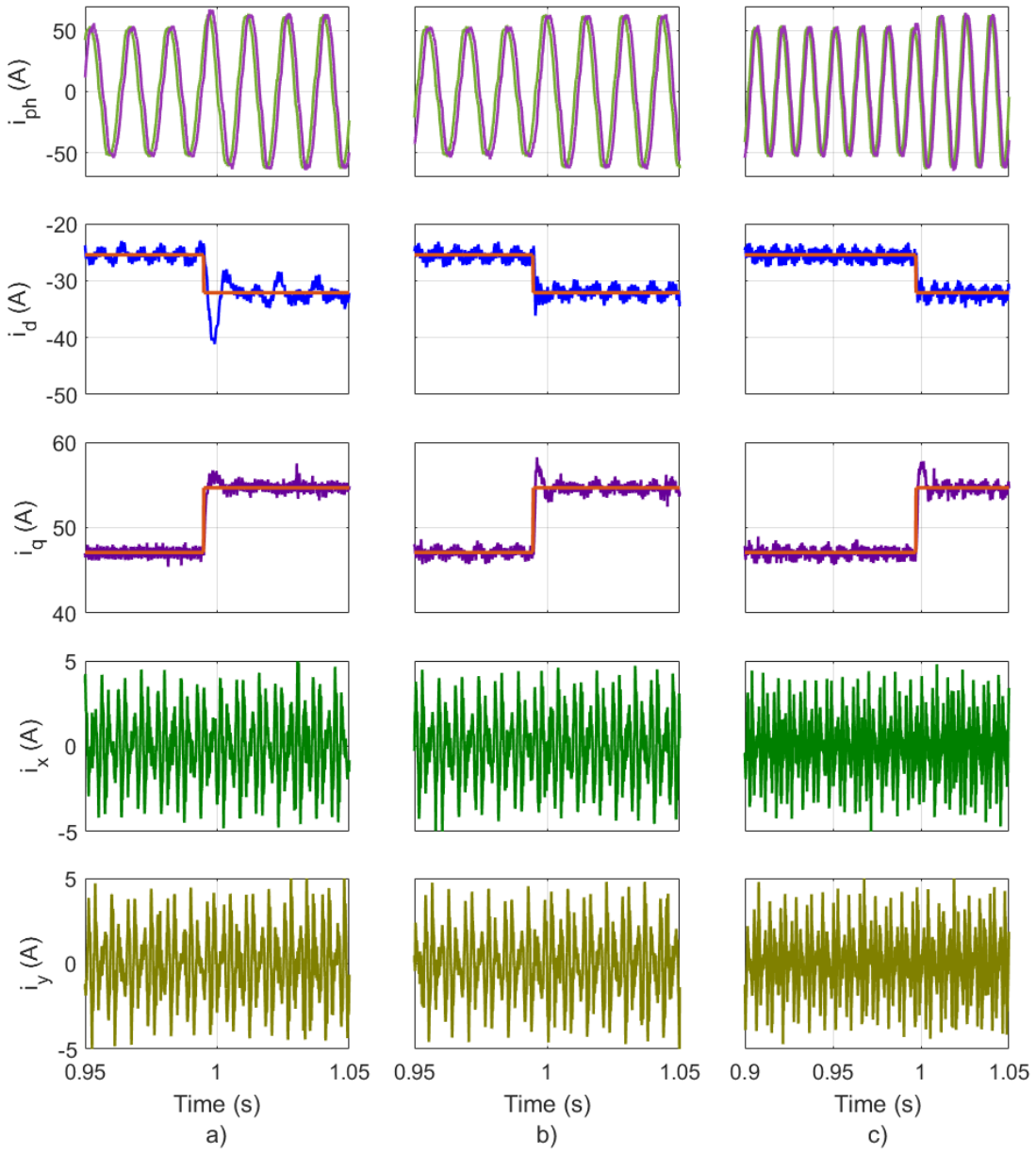

Figure 4.5: Step Response of: a) PI, b) Inductance Dynamic MPC c) Flux Dynamic MPC at 1000 rpm

4.3.4 Step-Change with Parameter Error

The other important test that was performed was the affect of modelling errors on the system. As discussed before, the dynamic MPC algorithms have an integral action embedded into the form. Therefore, it should have some degree of tolerance to modelling errors. From the simulations presented in chapter 3, it was decided to not test the parameter errors on the conventional model as it was thought that the erratic behaviour could damage the setup. It was decided to test this during a step change as with the error in the parameters the decoupling control of the PI controller would be most affected. A 1.2 percent error was applied to the inductance's as well as the permanent magnet flux linkage, and the step-change was applied again. The results of the experiment can be seen in Fig. 4.6 and table 4.5. As seen in the results, even with errors in the parameters, all of the algorithms are able to track the reference changes with little error. This is especially important with model predictive control as it is dependent on the model of the machine. However, overall, the results seem to show the same trends as the original step change experiment; the PI controller has some delay in the d current response and the MPC algorithms have a lower rise and fall time. Another important thing of note is that even with the parameter error, the flux-based MPC had a better performance compared to the inductance based version. It had lower ITSE values as well as quicker rise and fall times.

Table 4.5: Comparison of Step Response Results with 1.2 percent error

Control Strategy	**Speed**	**ISEd**	**ISEq**	**ISEx**	**ISEy**	**Fall Time id (ms)**	**Rise Time iq (ms)**
PI	1000	1.404	0.285	4.776	4.712	1.012	1.079
	1500	3.509	0.517	12.791	12.690	3.3616	1.0785
Inductance Dynamic MPC	1000	1.251	0.394	4.881	4.742	0.1212	0.8330
	1500	1.941	0.437	10.540	10.616	0.1391	0.6510
Flux Dynamic MPC	1000	1.226	0.392	4.982	4.938	0.1294	0.4613
	1500	1.875	0.424	10.421	10.544	0.2163	0.5302

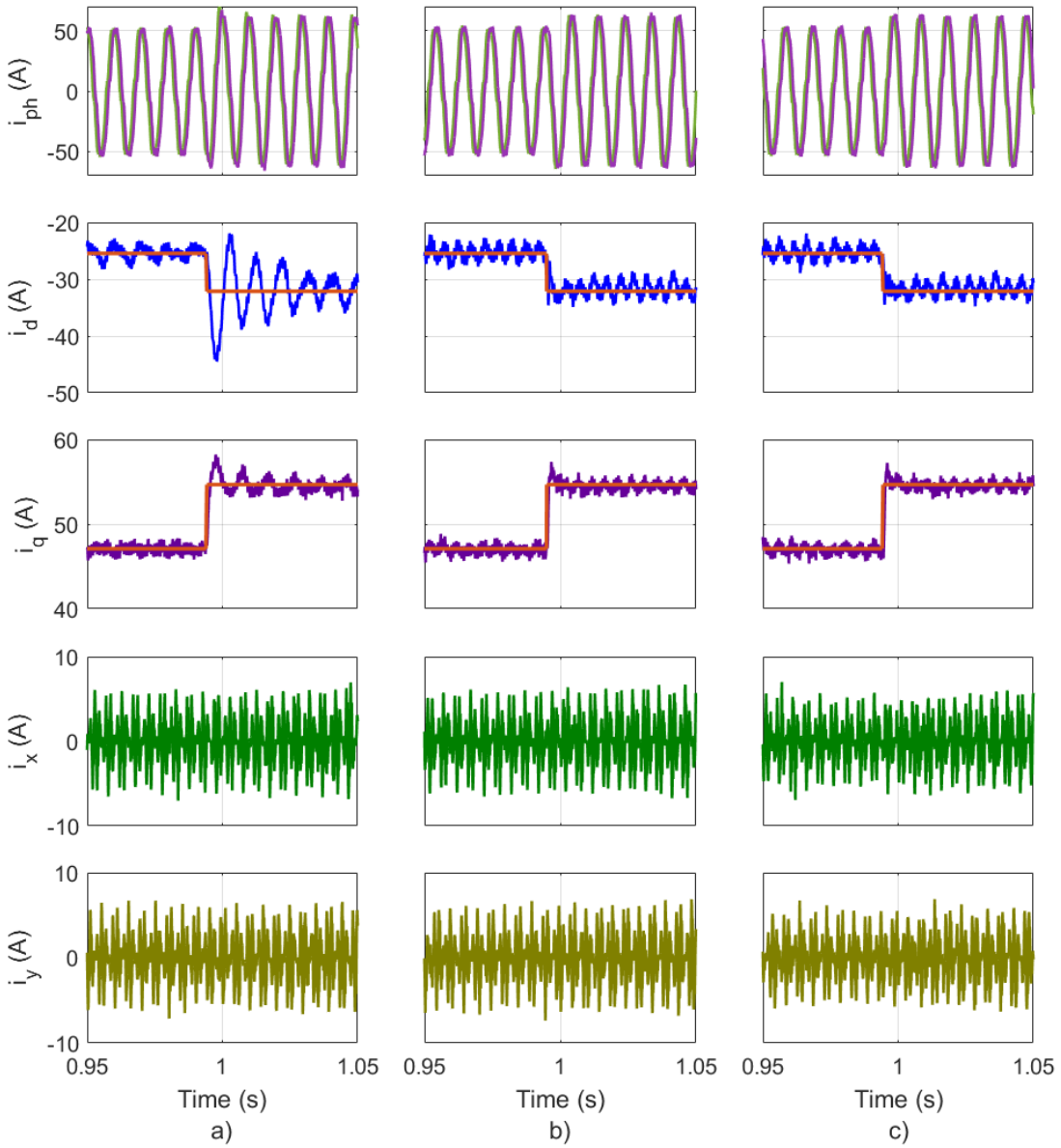

Figure 4.6: Step Response of: a) PI, b) Inductance Dynamic MPC c) Flux Dynamic MPC with 1.2 percent parameter error at 1500 rpm

Chapter 5

Conclusions and Future Work

The goal of this thesis was to present an improved model predictive control algorithm for the control of dual-three phase machines. As seen in the previous results, using the flux model for the machine in the conventional algorithm can improve the precision of the basic algorithm. Furthermore, by enhancing the algorithm with a dynamic subspace, the steady-state and step response results can be significantly improved.

There are a couple aspects of the algorithm that can be improved in the future. One aspect is the control of the xy currents. As discussed before, when the MPC algorithm was applied to the dqxy currents. It could control every current very well except for the xy current. This means that the basic model is not suited for modelling the x current. Further efforts should be made at creating a better model for the machine to compensate for this. One could investigate the use of dynamic inductance's for all subspaces or the use of the double dq transformation instead of the VSD. Furthermore, one could extend the dynamic subspace to other applications such as multilevel inverters or other multi-phase machines where FCS-MPC is commonly employed.

All in all, this thesis demonstrates that the improvements made to the finite-control set model predictive control algorithm. In general, researchers should continue to investigate new technologies and try to push the limits of what is currently available. This will make electric motors and electric vehicles better in the future, which will help alleviate the affects of climate change as a whole.

References and Bibliography

[Liu et al.(2020)Liu, Tu, Lin, and Liu] S.-M. Liu, C.-H. Tu, C.-L. Lin, and V.-T. Liu, "Field-Oriented Driving/Braking Control for Electric Vehicles," *Electronics*, vol. 9, no. 9, p. 1484, Sep. 2020, number: 9 Publisher: Multidisciplinary Digital Publishing Institute. [Online]. Available: https://www.mdpi.com/2079-9292/9/9/1484

[Nahid-Mobarakeh(2020)] B. Nahid-Mobarakeh, "Vector Control of PMSM," McMaster University, Oct. 2020.

[Narimani(2021)] M. Narimani, "Topic 5: Two-Level Voltage Source Inverter," McMaster University, Nov. 2021.

[Agnihotri et al.(2021)Agnihotri, Valencia, Taha, and Nahid-Mobarakeh] W. Agnihotri, D. F. Valencia, W. Taha, and B. Nahid-Mobarakeh, "Virtual-Flux Finite Control Set Model Predictive Control of Dual-Three Phase IPMSM Drives," in *IECON 2021 – 47th Annual Conference of the IEEE Industrial Electronics Society*, Oct. 2021, pp. 1–6, iSSN: 2577-1647.

[Hidrue et al.(2011)Hidrue, Parsons, Kempton, and Gardner] M. K. Hidrue, G. R. Parsons, W. Kempton, and M. P. Gardner, "Willingness to pay for

electric vehicles and their attributes," *Resource and Energy Economics*, vol. 33, no. 3, pp. 686–705, Sep. 2011. [Online]. Available: https://linkinghub.elsevier.com/retrieve/pii/S0928765511000200

[Ekta Bibra et al.(2021)Ekta Bibra, Connelly, Gorner, Lowans, Paoli, Tattini, and Teter] Ekta Bibra, E. Connelly, M. Gorner, C. Lowans, L. Paoli, J. Tattini, and J. Teter, "Global EV Outlook 2021," International Energy Agency, Tech. Rep., 2021. [Online]. Available: https://www.iea.org/reports/global-ev-outlook-2021

[Barzkar and Ghassemi(2020)] A. Barzkar and M. Ghassemi, "Electric Power Systems in More and All Electric Aircraft: A Review," *IEEE Access*, vol. 8, pp. 169 314–169 332, 2020, conference Name: IEEE Access.

[Li and Curiac(2011)] H. Li and R. Curiac, "Understanding of induction motors made easy," in *2011 Record of Conference Papers Industry Applications Society 58th Annual IEEE Petroleum and Chemical Industry Conference (PCIC)*, Sep. 2011, pp. 1–6, iSSN: 2161-8127.

[Bhatt et al.(2019)Bhatt, Mehar, and Sahajwani] P. Bhatt, H. Mehar, and M. Sahajwani, "Electrical Motors for Electric Vehicle – A Comparative Study," Social Science Research Network, Rochester, NY, SSRN Scholarly Paper 3364887, Apr. 2019. [Online]. Available: https://papers.ssrn.com/abstract=3364887

[Hashemnia and Asaei(2008)] N. Hashemnia and B. Asaei, "Comparative study of using different electric motors in the electric vehicles," in *2008 18th International Conference on Electrical Machines*, Sep. 2008, pp. 1–5.

[Moon et al.(2016)Moon, Lee, Jeong, and Kim] S. Moon, J. Lee, H. Jeong, and S. W. Kim, "Demagnetization fault diagnosis of a PMSM based on structure analysis of motor inductance," *IEEE Transactions on Industrial Electronics*, vol. 63, no. 6, pp. 3795–3803, Jun. 2016.

[Levi(2008)] E. Levi, "Multiphase Electric Machines for Variable-Speed Applications," *IEEE Transactions on Industrial Electronics*, vol. 55, no. 5, pp. 1893–1909, May 2008, conference Name: IEEE Transactions on Industrial Electronics.

[Salem and Narimani(2019)] A. Salem and M. Narimani, "A review on multiphase drives for automotive traction applications," *IEEE Transactions on Transportation Electrification*, pp. 1–1, 2019.

[Bojoi et al.(2018)Bojoi, Boggero, Comino, Fioriti, Tenconi, and Vaschetto] R. Bojoi, L. Boggero, S. Comino, M. Fioriti, A. Tenconi, and S. Vaschetto, "Multiphase Drives for Hybrid-Electric Propulsion in Light Aircrafts: a Viable Solution," in *2018 International Symposium on Power Electronics, Electrical Drives, Automation and Motion (SPEEDAM)*, Jun. 2018, pp. 613–619.

[Liu et al.(2021)Liu, Chau, Lee, and Song] C. Liu, K. T. Chau, C. H. T. Lee, and Z. Song, "A critical review of advanced electric machines and control strategies for electric vehicles," *Proceedings of the IEEE*, vol. 109, no. 6, pp. 1004–1028, Jun. 2021.

[Taylor et al.(2021)Taylor, Valencia Garcia, Taha, Mohamadian, Luedtke, Nahid-Mobarakeh, Bilgi
J. Taylor, D. F. Valencia Garcia, W. Taha, M. Mohamadian, D. Luedtke,

B. Nahid-Mobarakeh, B. Bilgin, and A. Emadi, "Dynamic modelling of multiphase machines based on the VSD transformation," *SAE Int. J. Adv. & Curr. Practices in Mobility*, vol. 3, no. 4, pp. 1620–1631, 2021.

[Hadiouche et al.(2006)Hadiouche, Baghli, and Rezzoug] D. Hadiouche, L. Baghli, and A. Rezzoug, "Space-vector PWM techniques for dual three-phase AC machine: analysis, performance evaluation, and DSP implementation," *IEEE Transactions on Industry Applications*, vol. 42, no. 4, pp. 1112–1122, Jul. 2006.

[Tenconi et al.(2018)Tenconi, Rubino, and Bojoi] A. Tenconi, S. Rubino, and R. Bojoi, "Model predictive control for multiphase motor drives – a technology status review," in *2018 International Power Electronics Conference (IPEC-Niigata 2018 -ECCE Asia)*, May 2018, pp. 732–739.

[Schwenzer et al.(2021)Schwenzer, Ay, Bergs, and Abel] M. Schwenzer, M. Ay, T. Bergs, and D. Abel, "Review on model predictive control: an engineering perspective," *The International Journal of Advanced Manufacturing Technology*, vol. 117, no. 5, pp. 1327–1349, Nov. 2021. [Online]. Available: https://doi.org/10.1007/s00170-021-07682-3

[Rodriguez and Cortes(2012)] J. Rodriguez and P. Cortes, *Predictive Control of Power Converters and Electrical Drives*, 1st ed. Chichester, West Sussex, UK ; Hoboken, N.J: Wiley-IEEE Press, Apr. 2012.

[Gonçalves et al.(2019)Gonçalves, Cruz, and Mendes] P. Gonçalves, S. Cruz, and A. Mendes, "Finite control set model predictive control of six-phase asymmetrical machines—An Overview," *Energies*, vol. 12, no. 24, p. 4693, Jan. 2019.

[Liu et al.(2018-06)Liu, Li, and Zheng] Z. Liu, Y. Li, and Z. Zheng, "A review of drive techniques for multiphase machines," *CES Transactions on Electrical Machines and Systems*, vol. 2, no. 2, pp. 243–251, 2018-06, conference Name: CES Transactions on Electrical Machines and Systems.

[Michalowicz(1948)] J. C. Michalowicz, "Origin of the electric motor," *Electrical Engineering*, vol. 67, no. 11, pp. 1035–1040, Nov. 1948, conference Name: Electrical Engineering.

[Ajanovic(2015)] A. Ajanovic, "The future of electric vehicles: prospects and impediments," *WIREs Energy and Environment*, vol. 4, no. 6, pp. 521–536, 2015, _eprint: https://onlinelibrary.wiley.com/doi/pdf/10.1002/wene.160. [Online]. Available: https://onlinelibrary.wiley.com/doi/abs/10.1002/wene.160

[Ewing(2022)] J. Ewing, "U.S. Electric Car Sales Climb Sharply Despite Shortages," *The New York Times*, Jul. 2022. [Online]. Available: https://www.nytimes.com/2022/07/14/business/electric-car-sales.html

[Murakami et al.(1999)Murakami, Honda, Kiriyama, Morimoto, and Takeda] H. Murakami, Y. Honda, H. Kiriyama, S. Morimoto, and Y. Takeda, "The performance comparison of SPMSM, IPMSM and SynRM in use as air-conditioning compressor," in *Conference Record of the 1999 IEEE Industry Applications Conference. Thirty-Forth IAS Annual Meeting (Cat. No.99CH36370)*, vol. 2, Oct. 1999, pp. 840–845 vol.2, iSSN: 0197-2618.

[Zhao and Lipo(1995)] Y. Zhao and T. Lipo, "Space vector PWM control of dual

three-phase induction machine using vector space decomposition," *IEEE Transactions on Industry Applications*, vol. 31, no. 5, pp. 1100–1109, Sep. 1995, conference Name: IEEE Transactions on Industry Applications.

[Hu et al.(2014)Hu, Zhu, and Liu] Y. Hu, Z.-Q. Zhu, and K. Liu, "Current Control for Dual Three-Phase Permanent Magnet Synchronous Motors Accounting for Current Unbalance and Harmonics," *IEEE Journal of Emerging and Selected Topics in Power Electronics*, vol. 2, no. 2, pp. 272–284, Jun. 2014, conference Name: IEEE Journal of Emerging and Selected Topics in Power Electronics.

[Duran et al.(2017)Duran, Gonzalez-Prieto, Barrero, Levi, Zarri, and Mengoni] M. J. Duran, I. Gonzalez-Prieto, F. Barrero, E. Levi, L. Zarri, and M. Mengoni, "A Simple Braking Method for Six-Phase Induction Motor Drives With Unidirectional Power Flow in the Base-Speed Region," *IEEE Transactions on Industrial Electronics*, vol. 64, no. 8, pp. 6032–6041, Aug. 2017, conference Name: IEEE Transactions on Industrial Electronics.

[Wang(2009)] L. Wang, *Model Predictive Control System Design and Implementation Using MATLAB®*, ser. Advances in Industrial Control. London: Springer London, 2009, iSSN: 1430-9491. [Online]. Available: http://link.springer.com/10.1007/978-1-84882-331-0

[Cortes et al.(2012)Cortes, Rodriguez, Silva, and Flores] P. Cortes, J. Rodriguez, C. Silva, and A. Flores, "Delay Compensation in Model Predictive Current Control of a Three-Phase Inverter," *IEEE Transactions on Industrial Electronics*, vol. 59, no. 2, pp. 1323–1325, Feb. 2012.

[Vaclavek and Blaha(2013-12)] P. Vaclavek and P. Blaha, "PMSM model discretization for model predictive control algorithms," in *Proceedings of the 2013 IEEE/SICE International Symposium on System Integration*, 2013-12, pp. 13–18.

[Burkhart et al.(2017)Burkhart, Klein-Hessling, Ralev, Weiss, and Doncker] B. Burkhart, A. Klein-Hessling, I. Ralev, C. P. Weiss, and R. W. D. Doncker, "Technology, research and applications of switched reluctance drives," *CPSS Transactions on Power Electronics and Applications*, vol. 2, no. 1, pp. 12–27, 2017.

[Hepp et al.(2020-08)Hepp, Imamovic, Wondrak, and Parspour] M. Hepp, D. Imamovic, W. Wondrak, and N. Parspour, "Predictive high dynamic current control of dual three-phase PMSMs," in *2020 International Conference on Electrical Machines (ICEM)*, vol. 1, 2020-08, pp. 2139–2144, ISSN: 2381-4802.

[Zhang et al.(2018-08)Zhang, Bai, and Yang] Y. Zhang, Y. Bai, and H. Yang, "A universal multiple-vector-based model predictive control of induction motor drives," *IEEE Transactions on Power Electronics*, vol. 33, no. 8, pp. 6957–6969, 2018-08, conference Name: IEEE Transactions on Power Electronics.

[Khader and Nahla(2021-04)] S. Khader and M. A. Nahla, "Model predictive current control with duty ratio optimization for three phase grid-tie micro inverter based on runge kutta approximation," in *2021 12th International Renewable Engineering Conference (IREC)*, 2021-04, pp. 1–7.

[Pevec et al.(2019)Pevec, Babic, and Podobnik] D. Pevec, J. Babic, and V. Podobnik, "Electric vehicles: A data science perspective review," *Electronics*, vol. 8,

no. 10, p. 1190, 2019, number: 10 Publisher: Multidisciplinary Digital Publishing Institute. [Online]. Available: https://www.mdpi.com/2079-9292/8/10/1190

[Karamanakos et al.(2014-03)Karamanakos, Geyer, Oikonomou, Kieferndorf, and Manias] P. Karamanakos, T. Geyer, N. Oikonomou, F. D. Kieferndorf, and S. Manias, "Direct model predictive control: A review of strategies that achieve long prediction intervals for power electronics," *IEEE Industrial Electronics Magazine*, vol. 8, no. 1, pp. 32–43, 2014-03, conference Name: IEEE Industrial Electronics Magazine.

[Andersson and Thiringer(2020-01)] A. Andersson and T. Thiringer, "Assessment of an improved finite control set model predictive current controller for automotive propulsion applications," *IEEE Transactions on Industrial Electronics*, vol. 67, no. 1, pp. 91–100, 2020-01, conference Name: IEEE Transactions on Industrial Electronics.

[Hammoud et al.(2020-10)Hammoud, Hentzelt, Oehlschlaegel, and Kennel] I. Hammoud, S. Hentzelt, T. Oehlschlaegel, and R. Kennel, "Long-horizon direct model predictive control based on neural networks for electrical drives," in *IECON 2020 The 46th Annual Conference of the IEEE Industrial Electronics Society*, 2020-10, pp. 3057–3064, ISSN: 2577-1647.

[Liu and Liu(2021)] S. Liu and C. Liu, "Virtual-vector-based robust predictive current control for dual three-phase PMSM," *IEEE Transactions on Industrial Electronics*, vol. 68, no. 3, pp. 2048–2058, Mar. 2021.

[Rodríguez et al.(2020)Rodríguez, Heydari, Rafiee, Young, Flores-Bahamonde, and Shahparasti] J. Rodríguez, R. Heydari, Z. Rafiee, H. A. Young, F. Flores-Bahamonde, and

M. Shahparasti, "Model-free predictive current control of a voltage source inverter," *IEEE Access*, vol. 8, pp. 211 104–211 114, 2020, conference Name: IEEE Access.

[Yuan et al.(2020-12)Yuan, Ma, Zhao, and Yang] Q. Yuan, T. Ma, R. Zhao, and Y. Yang, "A general double vector-based model predictive current control for the dual three-phase motors," *Electronics*, vol. 9, no. 12, p. 2000, 2020-12, number: 12 Publisher: Multidisciplinary Digital Publishing Institute. [Online]. Available: https://www.mdpi.com/2079-9292/9/12/2000

[Gonçalves et al.(2019-02a)Gonçalves, Cruz, and Mendes] P. F. C. Gonçalves, S. M. A. Cruz, and A. M. S. Mendes, "Predictive current control based on variable amplitude virtual vectors for six-phase permanent magnet synchronous machines," in *2019 IEEE International Conference on Industrial Technology (ICIT)*, 2019-02, pp. 310–316, ISSN: 2643-2978.

[Gonçalves et al.(2019-02b)Gonçalves, Cruz, and Mendes] ——, "Predictive current control based on variable amplitude virtual vectors for six-phase permanent magnet synchronous machines," in *2019 IEEE International Conference on Industrial Technology (ICIT)*, 2019-02, pp. 310–316, ISSN: 2643-2978.

[Gonçalves et al.(2019)Gonçalves, Cruz, and Mendes] ——, "Bi-subspace predictive current control of six-phase PMSM drives based on virtual vectors with optimal amplitude," *IET Electric Power Applications*, vol. 13, no. 11, pp. 1672–1683, 2019, _eprint: https://ietresearch.onlinelibrary.wiley.com/doi/pdf/10.1049/iet-epa.2019.0136. [Online]. Available: https://onlinelibrary.wiley.com/doi/abs/10.1049/iet-epa.2019.0136

[Duran et al.(2011-08)Duran, Prieto, Barrero, and Toral] M. J. Duran, J. Prieto, F. Barrero, and S. Toral, "Predictive current control of dual three-phase drives using restrained search techniques," *IEEE Transactions on Industrial Electronics*, vol. 58, no. 8, pp. 3253–3263, 2011-08, conference Name: IEEE Transactions on Industrial Electronics.

[Sahin and Keysan(2018-04)] I. Sahin and O. Keysan, "A new model predictive torque control strategy with reduced set of prediction vectors," in *2018 IEEE 12th International Conference on Compatibility, Power Electronics and Power Engineering (CPE-POWERENG 2018)*, 2018-04, pp. 1–6, ISSN: 2166-9546.

[Gonzalez-Prieto et al.(2022)Gonzalez-Prieto, Martin, González-Prieto, Duran, Carrillo-Ríos, and A
A. Gonzalez-Prieto, C. Martin, I. González-Prieto, M. J. Duran, J. Carrillo-Ríos, and J. J. Aciego, "Hybrid Multivector FCS–MPC for Six-Phase Electric Drives," *IEEE Transactions on Power Electronics*, vol. 37, no. 8, pp. 8988–8999, Aug. 2022, conference Name: IEEE Transactions on Power Electronics.

[Cortes et al.(2009-02)Cortes, Kouro, La Rocca, Vargas, Rodriguez, Leon, Vazquez, and Franquelo
P. Cortes, S. Kouro, B. La Rocca, R. Vargas, J. Rodriguez, J. I. Leon, S. Vazquez, and L. G. Franquelo, "Guidelines for weighting factors design in model predictive control of power converters and drives," in *2009 IEEE International Conference on Industrial Technology*, 2009-02, pp. 1–7.

[Villarroel et al.(2013-02)Villarroel, Espinoza, Rojas, Rodriguez, Rivera, and Sbarbaro]
F. Villarroel, J. R. Espinoza, C. A. Rojas, J. Rodriguez, M. Rivera, and D. Sbarbaro, "Multiobjective switching state selector for finite-states model predictive

control based on fuzzy decision making in a matrix converter," *IEEE Transactions on Industrial Electronics*, vol. 60, no. 2, pp. 589–599, 2013-02, conference Name: IEEE Transactions on Industrial Electronics.

[Fretes et al.(2022)Fretes, Rodas, Doval-Gandoy, Gomez, Gomez, Novak, Rodriguez, and Dragičevi H. Fretes, J. Rodas, J. Doval-Gandoy, V. Gomez, N. Gomez, M. Novak, J. Rodriguez, and T. Dragičević, "Pareto Optimal Weighting Factor Design of Predictive Current Controller of a Six-Phase Induction Machine Based on Particle Swarm Optimization Algorithm," *IEEE Journal of Emerging and Selected Topics in Power Electronics*, vol. 10, no. 1, pp. 207–219, Feb. 2022, conference Name: IEEE Journal of Emerging and Selected Topics in Power Electronics.

[Sheng et al.(2018-05-31)Sheng, Li, and Ji] L. Sheng, D. Li, and Y. Ji, "Two-vector FCS-MPC for permanent-magnet synchronous motors based on duty ratio optimization," *Mathematical Problems in Engineering*, vol. 2018, p. e9061979, 2018-05-31, publisher: Hindawi. [Online]. Available: https://www.hindawi.com/journals/mpe/2018/9061979/

[Norambuena et al.(2019-12)Norambuena, Lezana, and Rodriguez] M. Norambuena, P. Lezana, and J. Rodriguez, "A method to eliminate steady-state error of model predictive control in power electronics," *IEEE Journal of Emerging and Selected Topics in Power Electronics*, vol. 7, no. 4, pp. 2525–2530, 2019-12, conference Name: IEEE Journal of Emerging and Selected Topics in Power Electronics.

[Yang et al.(2016-03)Yang, Tan, and Hui] Y. Yang, S.-C. Tan, and S.-Y. Hui, "Adaptive reference model predictive control for power electronics," in *2016 IEEE Applied Power Electronics Conference and Exposition (APEC)*, 2016-03, pp. 1169–1175.

[Wendel et al.(2021-12)Wendel, Karamanakos, Gebhardt, Dietz, and Kennel] S. Wendel, P. Karamanakos, P. Gebhardt, A. Dietz, and R. Kennel, "Flux linkage-based direct model predictive current control for synchronous machines," *IEEE Transactions on Power Electronics*, vol. 36, no. 12, pp. 14 237–14 256, 2021-12, conference Name: IEEE Transactions on Power Electronics.

[Wang et al.(2021-06)Wang, Liu, Liu, and Zhao] W. Wang, C. Liu, S. Liu, and H. Zhao, "Model predictive torque control for dual three-phase PMSMs with simplified deadbeat solution and discrete space-vector modulation," *IEEE Transactions on Energy Conversion*, vol. 36, no. 2, pp. 1491–1499, 2021-06, conference Name: IEEE Transactions on Energy Conversion.

[Alsofyani et al.(2019-03)Alsofyani, Kim, and Lee] I. M. Alsofyani, S.-M. Kim, and K.-B. Lee, "Finite set predictive torque control based on sub-divided voltage vectors of PMSM with deadbeat control and discrete space vector modulation," in *2019 IEEE Applied Power Electronics Conference and Exposition (APEC)*, 2019-03, pp. 1853–1857, ISSN: 2470-6647.

[Lee et al.(2018)Lee, Lee, Moon, and Lee] J.-H. Lee, J.-S. Lee, H.-C. Moon, and K.-B. Lee, "An Improved Finite-Set Model Predictive Control Based on Discrete Space Vector Modulation Methods for Grid-Connected Three-Level Voltage

Source Inverter," *IEEE Journal of Emerging and Selected Topics in Power Electronics*, vol. 6, no. 4, pp. 1744–1760, Dec. 2018, conference Name: IEEE Journal of Emerging and Selected Topics in Power Electronics.

[Preindl(2016)] M. Preindl, "Robust control invariant sets and lyapunov-based MPC for IPM synchronous motor drives," *IEEE Transactions on Industrial Electronics*, vol. 63, no. 6, pp. 3925–3933, 2016.

[Taha et al.(2018)Taha, Beig, and Boiko] W. Taha, A. R. Beig, and I. Boiko, "Quasi optimum PI controller tuning rules for a grid-connected three phase AC to DC PWM rectifier," *Int. J. Electr. Power Energy Syst.*, vol. 96, pp. 74–85, Mar. 2018.

[Rao(2009)] S. S. Rao, "Nonlinear programming II: Unconstrained optimization techniques," in *Engineering optimization theory and practice*, 4th ed. Hoboken, NJ: John Wiley & Sons, 2009, ch. 6, pp. 301–379.